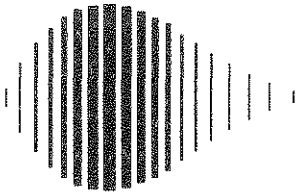

NATIONAL CENTER FOR EARTHQUAKE
ENGINEERING RESEARCH
State University of New York at Buffalo

TWO- AND THREE-DIMENSIONAL DYNAMIC FINITE ELEMENT ANALYSES OF THE LONG VALLEY DAM

by

D.V. Griffiths and J.H. Prevost
Department of Civil Engineering and Operations Research
Princeton University
Princeton, New Jersey 08544

Technical Report NCEER-88-0015

June 17, 1988

This research was conducted at Princeton University and was partially supported by the National Science Foundation under Grant No. ECE 86-07591.

NOTICE

This report was prepared by Princeton University as a result of research sponsored by the National Center for Earthquake Engineering Research (NCEER). Neither NCEER, associates of NCEER, its sponsors, Princeton University, or any person acting on their behalf:

a. makes any warranty, express or implied, with respect to the use of any information, apparatus, method, or process disclosed in this report or that such use may not infringe upon privately owned rights; or

b. assumes any liabilities of whatsoever kind with respect to the use of, or for damages resulting from the use of, any information, apparatus, method or process disclosed in this report.

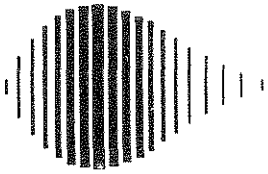

TWO- AND THREE-DIMENSIONAL DYNAMIC FINITE ELEMENT ANALYSES OF THE LONG VALLEY DAM

by

D.V. Griffiths[1] and J.H. Prevost[2]

June 17, 1988

Technical Report NCEER-88-0015

NCEER Contract Number 86-3034

NSF Master Contract Number ECE 86-07591

NSF Grant Number ECE 85-12311

1 Research Fellow and Senior Fulbright Scholar, University of Manchester, U.K.
2 Professor, Department of Civil Engineering, Princeton University

NATIONAL CENTER FOR EARTHQUAKE ENGINEERING RESEARCH
State University of New York at Buffalo
Red Jacket Quadrangle, Buffalo, NY 14261

PREFACE

The National Center for Earthquake Engineering Research (NCEER) is devoted to the expansion and dissemination of knowledge about earthquakes, the improvement of earthquake-resistant design, and the implementation of seismic hazard mitigation procedures to minimize loss of lives and property. The emphasis is on structures and lifelines that are found in zones of moderate to high seismicity throughout the United States.

NCEER's research is being carried out in an integrated and coordinated manner following a structured program. The current research program comprises four main areas:

- Existing and New Structures
- Secondary and Protective Systems
- Lifeline Systems
- Disaster Research and Planning

This technical report pertains to Program 1, Existing and New Structures, and more specifically to geotechnical studies, soils and soil-structure interaction.

The long term goal of research in Existing and New Structures is to develop seismic hazard mitigation procedures through rational probabilistic risk assessment for damage or collapse of structures, mainly existing buildings, in regions of moderate to high seismicity. The work relies on improved definitions of seismicity and site response, experimental and analytical evaluations of systems response, and more accurate assessment of risk factors. This technology will be incorporated in expert systems tools and improved code formats for existing and new structures. Methods of retrofit will also be developed. When this work is completed, it should be possible to characterize and quantify societal impact of seismic risk in various geographical regions and large municipalities. Toward this goal, the program has been divided into five components, as shown in the figure below:

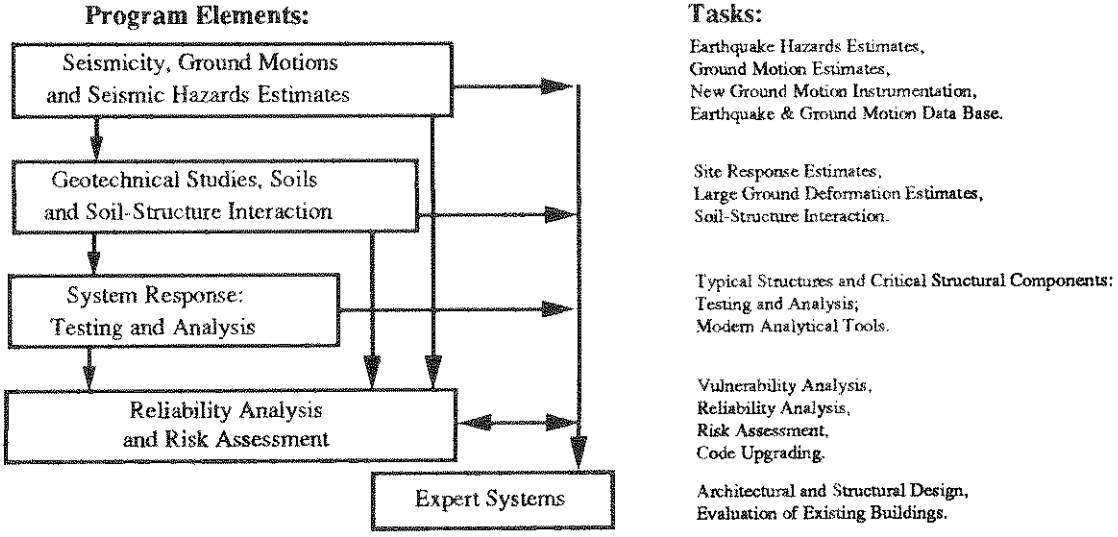

Geotechnical studies, soils and soil-structure interaction constitute one of the important areas of research in Existing and New Structures. Current research activities include the following:

1. Development of linear and nonlinear site response estimates.
2. Development of liquefaction and large ground deformation estimates.
3. Investigation of soil-structure interaction phenomena.
4. Development of computational methods.
5. Incorporation of local soil effects and soil-structure interaction into existing codes.

The ultimate goal of projects in this area is to develop methods of engineering estimation of large soil deformations, site response, and the effect that the interaction of structures and soils have on the resistance of structures against earthquakes.

This report presents the results of a study of earthquake response recorded on the Long Valley Dam in the Mammoth Lake area of California. A rigorous finite element analysis is used to reproduce the observed response, in which the nonlinear hysteretic behavior of the dam materials is accounted for by using a multi-surface plasticity theory.

ABSTRACT

Earthquake response records of the well-instrumented Long Valley Dam in the Mammoth Lake area of California are compared with numerical prediction made using finite element models. The soil response to cyclic loading is accounted for by the use of a multi-surface plasticity model [1]. The input and output to the finite element analyses take the form of accelerations at the base and at various crest locations. The computed and measured crest acceleration are compared in both the time and frequency domains. Natural frequencies have also been obtained for the finite element models and for the real structure from spectral analysis, and are in generally good agreement. The time-domain results give good agreement and high correlation in the up/down-stream direction but poor agreement in the vertical (and transverse in the case of 3-D) direction. The failure of the finite element models to capture the high-frequencies present in the vertical and transverse directions is thought to be partly due to the crude finite element discretisation used. To improve the modelling in these directions, a finer 3-D mesh has been prepared for further analysis and the results will be presented in a subsequent report.

Table of Contents

LIST OF ILLUSTRATIONS

LIST OF TABLES

SECTION 1

INTRODUCTION

The response of earth dams to earthquake excitation is a complex process in which full account must be taken of the non-linear response of the soil skeleton to cyclic loading. The form of the assumed constitutive relations for the soils will depend to a large extent on the type of materials present in the dam, and their relative permeabilities. In an earlier analysis on the Santa Felicia Dam [2], the embankments had a much higher permeability than the clay core resulting in a steeply falling free-surface line. The saturated materials below the free-surface were treated to a fully coupled finite element analysis in which account was taken of the two-phase nature of the soil/water mixture. The two-phase approach was found to give a better response than the equivalent one-phase approach when compared with measured values from the field.

The present paper describes finite element analyses of the Long Valley Dam which is constructed of an extensive rolled earthfill core, and has compacted embankments of more permeable material. The extensive nature of the clay core means that the free-surface falls very gradually through the dam, hence the entire dam is essentially saturated. A two-phase analysis in this case would be inappropriate, hence a one-phase approach is used in which the soil/water mixture is treated as a single composite material.

The Long Valley Dam [3] was constructed in the 1930's and was built in a narrow canyon approximately 35km northwest of the city of Bishop, California. The dam has a maximum height above the valley floor of 54m. In May 1980, the area was subjected to a series of earthquakes which triggered a number of accelerographs placed on or around the dam [4]. Figure 1-1 shows various sections of the dam and the location and orientation of the 22 accelerographs. The largest earthquake experienced by the dam occurred on May 27th 1980 resulting in peak acceleration in the x (up/downstream), y (vertical) and z (transverse) direction of 0.18g, 0.09g and 0.22g respectively. Acceleration readings were made at 0.02 sec intervals and a total duration of 12 secs was

used as input to the finite element analyses.

Previous analyses of the Long Valley Dam have been reported in [5]. In these analyses, the non-linear characteristics of the dam behavior were accounted for by using equivalent linear soil properties and an iterative procedure to obtain modulus and damping values compatible with the amount of straining computed in each zone of the soil mass. In the analyses reported herein, a more rigorous approach is used in which the nonlinear hysteretic behavior of the dam materials is accounted for by using a multi-surface plasticity theory [1]. All calculations reported herein were performed by using the computer code DYNAFLOW [6] developed at Princeton University.

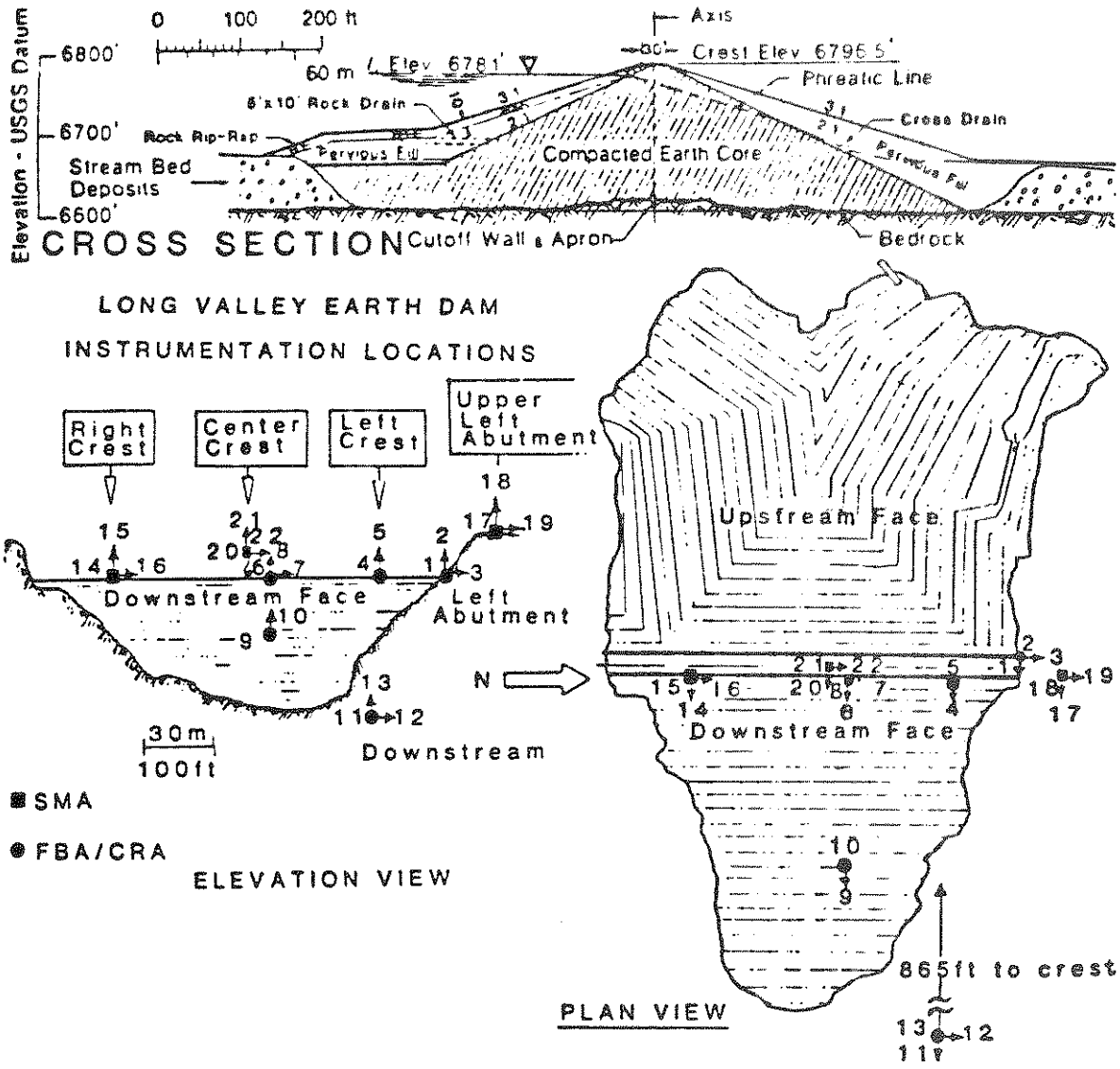

Fig. 1-1 General details of the Long Valley Dam and the location of strong motion instrumentation.

SECTION 2

FINITE ELEMENT DISCRETIZATION

2.1 Two-Dimensions

The widest section of the dam in the up/downstream direction was used as a basis for the 2-D finite element discretisation shown in Figure 2-1. The mesh has 215 nodes, 178 4-node elements and 352 degrees of freedom in the x- and y- direction. The mesh is divided into nine soil groups and each zone is given different soil properties to reflect the spatial variation in stiffness and strength. Two groups represent the embankment shell material, six groups represent the clay core and one group represents the existing stream beds to the sides. The input accelerations were applied in the x- and y- directions to the 39 nodes at the base and extreme sides of the mesh. The input was taken from the corresponding measured acceleration from accelerographs 11 and 13 (Figure 1-1). At each time step (Δt = 0.02sec) the x- and y- acceleration at all nodes in the mesh were computed from the non-linear finite element analysis. Of particular interest was the computed acceleration at the crest (node 111) which could be compared directly with measured values at accelerographs 20 and 21.

2.2 Three-Dimensions

The Long Valley Dam is build in a relatively narrow canyon, and it was felt that the assumption of plane-strain conditions at the centerline might not be wholly justified. For this reason, a three-dimensional model of the dam was created as shown in Figure 2-2. The mesh consists of 13 sections in the transverse direction, and is symmetrical about the up/downsteam centreline. The mesh consists of 878 nodes, 528 8-node brick elements and 1620 degrees of freedom in the x-, y- and z-directions. In spite of the greater number of elements, the mesh only contains five soil groups; one in the shell, three in the core and one to the sides. This was felt to be a rather crude description of the spatial variation of soil

properties. Input accelerations to the base and sides of the mesh were those recorded at stations 11, 13 and 12 respectively and computed accelerations at nodes 777, 49 and 383 (Figure 2-2) along the crest were compared with accelerograph readings obtained at stations 14 thru 16, 20 thru 22 and 4 thru 5.

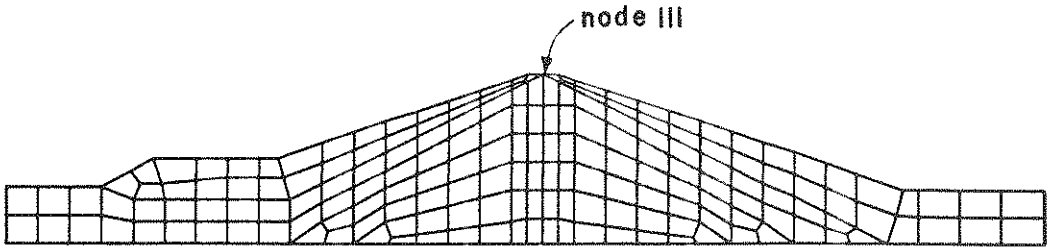

Fig.2-1 Mesh Used for 2-D Analyses.

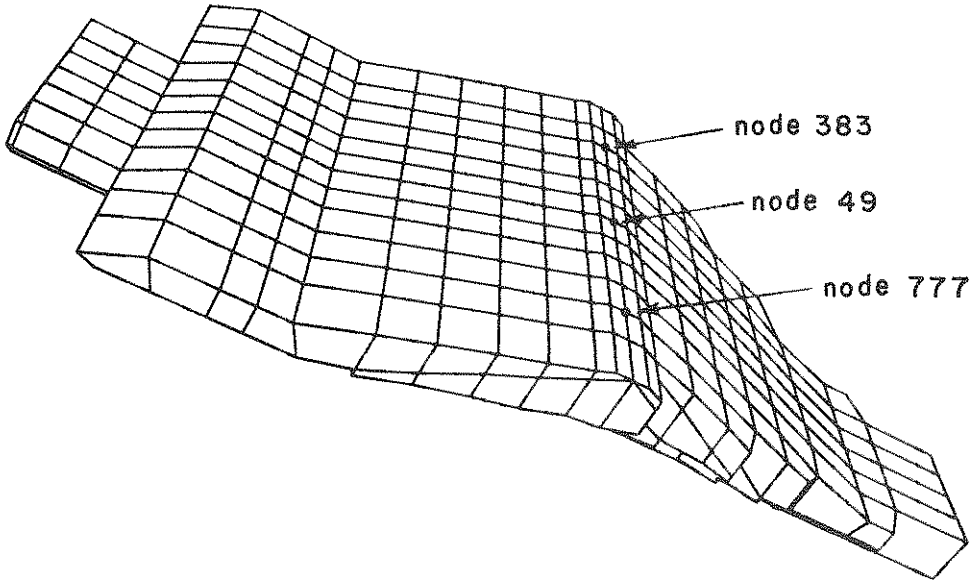

Fig.2-2 Mesh Used for 3-D Analyses.

SECTION 3

SOIL PROPERTIES

Tables 3-I and 3-II show the elastic properties and shear strength parameters assigned to each element group in the two and three-dimensional analyses. The moduli were related to the initial mean overburden pressure in each group which was obtained by multiplying the mean group depth by 20 kN / m^3 and assuming a value for the lateral earth pressure coefficient. The data shown in Tables 3.I and 3.II for the core were taken from a previous analysis [7] in which similar core materials were used. In the present case, the low-permeability clay core was assigned a higher Poisson's ratio of $\nu_o = 0.45$ than the relatively permeable shell material where $\nu_o = 0.3$.

The core material was assigned $K_o = 1$ whereas the shell was given a lower value more appropriate for granular materials where $K_o = 1 - \sin \phi'$. From the initial mean stress and shear stress within each group (p_o and q_o respectively) and the shear strength parameters c' and ϕ', a stress path could be assumed and the shear strength estimated. For the core material, an undrained triaxial stress path in which $dp/dq = 0$ (ie. no volume change tendency) was assumed, whereas for the more permeable shell, a drained triaxial stress path in which $dp/dq = 1/3$ was assumed.

Knowing the initial gradient and the ultimate strength, a stress/strain curve was then fitted to the data in both compression and extension. The usual method of doing this is to use a hyperbola of the form:

$$q = \frac{G_o \bar{\varepsilon}}{1 + \frac{G_o}{q_{max}} \bar{\varepsilon}} \tag{3.1}$$

An alternative logarithmic function has also been used in the 3-D analyses of the form:

$$\bar{\varepsilon} = Aq - B ln\left(1 - \frac{q}{q_{max}}\right) \tag{3.2}$$

which can be arranged to have the correct initial gradient G_o where:

$$G_o = \frac{q_{max}}{A\ q_{max} + B} \tag{3.3}$$

By varying A and B, the shape of the curve can be adjusted. It may be noted that stress/strain curve generation functions such as those given by equations (3.1) and (3.2) are no substitute for actual test data when available.

Having obtained the stress/strain curve in both compression and extension, a series of cylindrical yield surfaces [1] could then be generated for use in the multi-surface plasticity model. The present model includes no viscous damping, the main source of damping being hysteretic.

Table 3-I Material Properties for 2-D Long Valley Dam Analyses.

Group	E_0(kPa)	ν_0	ϕ'	c'(kPa)	
1	1.6E5	0.3	40	0	drained
2	2.1E5	0.3	40	0	drained
3	4.0E5	0.45	39	45	undrained
4	5.0E5	0.45	39	45	undrained
5	5.5E5	0.45	39	45	undrained
6	5.9E5	0.45	39	45	undrained
7	6.2E5	0.45	39	45	undrained
8	6.5E5	0.45	39	45	undrained
9	4.9E6	0.3			elastic

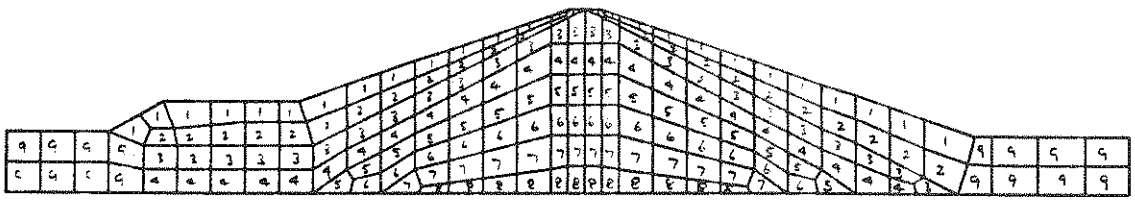

Table 3-II Material Properties for 3-D Long Valley Dam Analyses.

Group	E_0(kPa)	ν_0	ϕ'	c'(kPa)	
1	1.9E5	0.3	40	0	drained
2	4.3E5	0.45	39	45	undrained
3	5.5E5	0.45	39	45	undrained
4	6.3E5	0.45	39	45	undrained
5	4.9E6	0.3			elastic

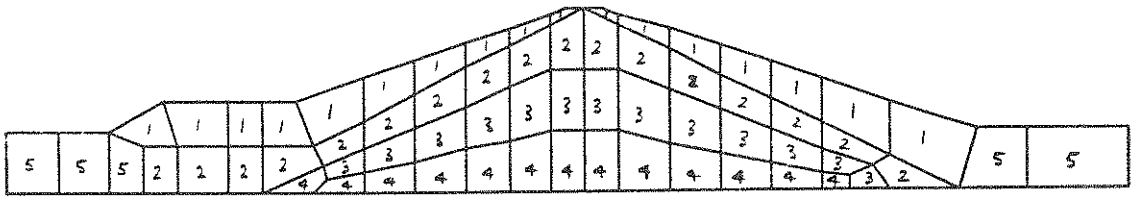

SECTION 4

NUMERICAL ALGORITHMS

The eigenvalue analyses were performed using a subspace iterations approach. The elastic properties indicated by Tables 3-I and 3-II were assigned to the mesh and the mass was lumped at the nodes assuming a density throughout of 2000 kg / m^3.

The non-linear time domain analyses used modified Newton-Raphson iterations with a reform at each time step together with a dimensionless convergence tolerance of 10^{-3}. A Newmark [8] time stepping algorithm was used for the time integrations, with a time stepping algorithm parameter of $\alpha = 0.55$, $\beta = 0.28$. The slight numerical damping introduced by these values was considered justified, as it would remove any spurious high frequencies present due to the finite element discretisation.

SECTION 5

EIGENVALUE ANALYSES

The results from the 2- and 3-D analyses are shown in Table 5-I. Only the first three natural frequencies are presented in each case, and these are compared with values estimated from spectral analysis of the response to earthquake excitation. The computed and measured values give acceptable agreement in both cases, although the 3-D values give closer agreement than the 2-D values. Figure 5-1 gives the first three 2-D mode shapes, and Figure 5-2 the first two 3-D mode shapes. (The 3rd mode shape in 3-D was not included because the 3-D plotter did not give a clear representation). The fundamental mode shape is clearly an upstream/downstream motion with a natural frequency in the range 1.75 Hz - 1.95 Hz, but it should be noted that the second and subsequent mode shapes are not necessarily the same in 2- and 3-D. For example from Figure 5-1b, the second 2-D mode shape implies an almost symmetrical vertical motion whereas the second 3-D mode shape from Figure 5-2b implies an antisymmetric vertical motion along the crest. Care must therefore be taken when comparing natural frequencies from different analyses.

Table 5-I Eigenvalue Analyses.

Mode number	Resonant frequencies from spectral analysis (Hz)	From 2-D FE model	From 3-D FE model
1	1.85	1.76	1.95
2	2.15	2.58	2.20
3	2.45	3.00	2.25

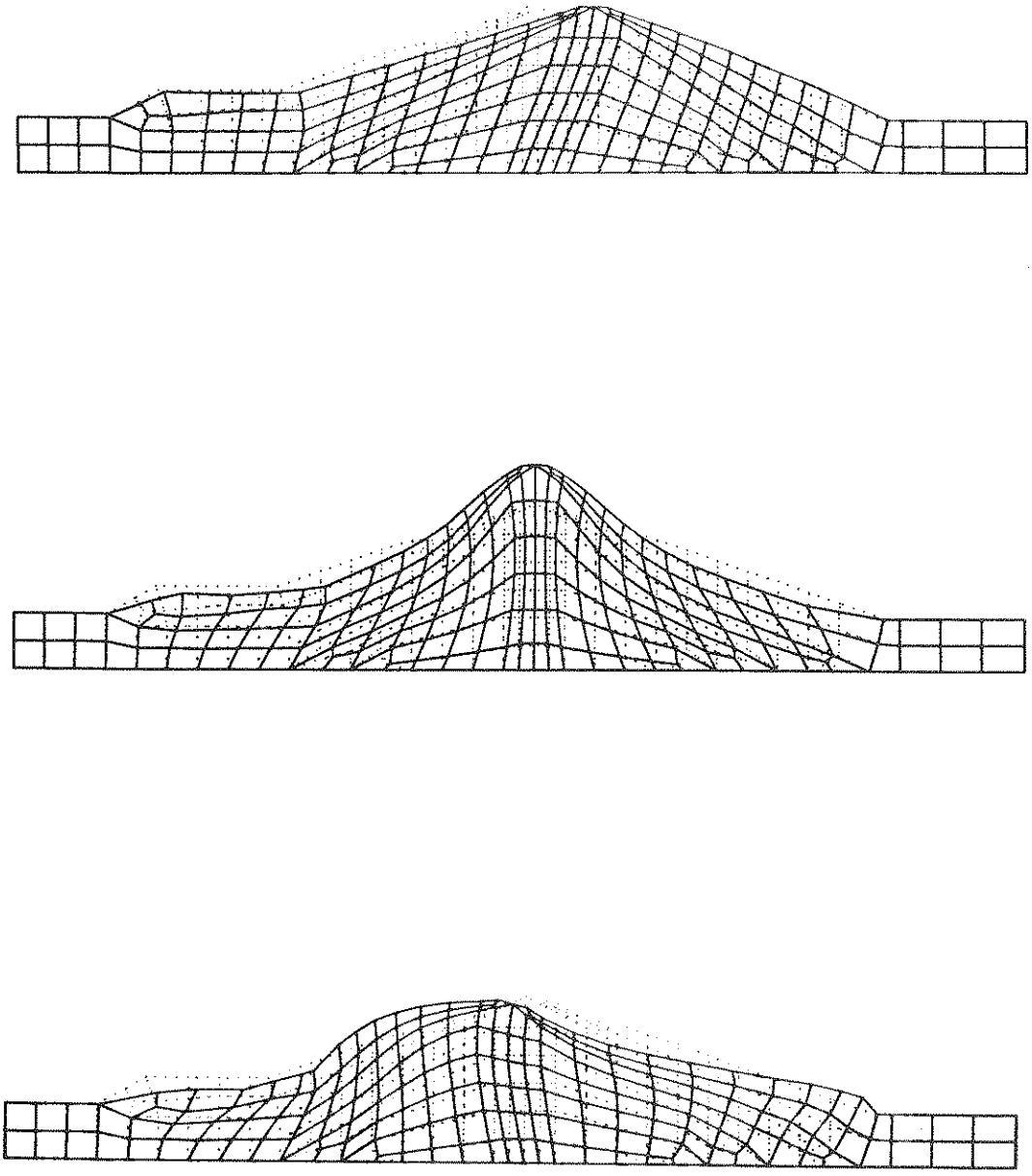

Fig.5-1 First Three 2-D Eigenmodes.

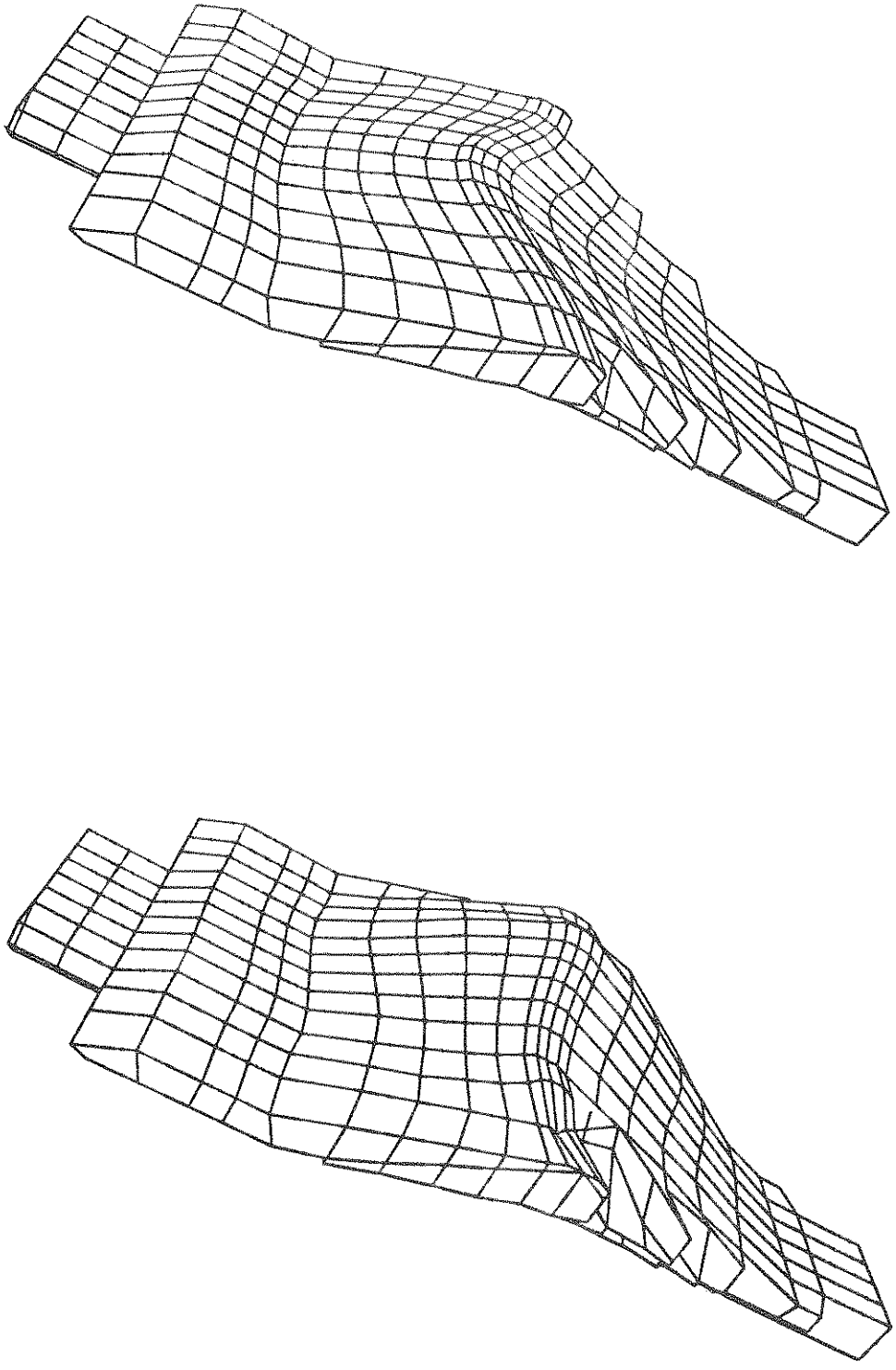

Fig.5-2 First Two 3-D Eigenmodes.

SECTION 6

TIME DOMAIN ANALYSES

6.1 Two Dimensions

The accelerographs took their reading at 0.02 sec intervals which was also selected to be the time step used in the numerical time stepping algorithm. Accelerations were applied uniformly to the base of the mesh over a period of 12 secs. (600 steps).

Figure 6-1 shows the x-acceleration as measured at stations 11 and 20 and indicates the amplification that has occurred between the base and the crest. The peak amplitude at the crest has a magnification factor of about 3 over the peak base amplitude. The computed response of the crest in the up/downstream direction is compared with measured values in Figure 6-2. Excellent overall agreement is achieved, with the computed values (solid lines) giving somewhat higher amplitudes. The frequency content of the two time records is compared in the form of a Fourier Amplitude Spectrum (FAS) in Figure 6-2b. The peaks are in close agreement although the computed values show rather more energy associated with the fundamental frequency around 1.8 Hz.

The response of a single degree of freedom oscillator with 10% damping to the computed and measured acceleration in the up/downstream direction is shown in Figure 6-2c in the form of a Velocity Response Spectrum (VRS). This plot gives the maximum velocity recorded as a function of the natural period of the oscillator. The curves are in close agreement and give similar information to that provided by the Fourier spectrum but in smoother form. An additional comparison of the two records was made by calculating the correlation coefficient r_{xy} where:

$$r_{xy} = \frac{s_{xy}}{s_{xx}\, s_{yy}} \tag{6.1}$$

$$s_{xx}^2 = \frac{1}{n}\sum_{i=1}^{n}(x_i - \bar{x})^2 \quad x - sample \;\; variance \tag{6.2}$$

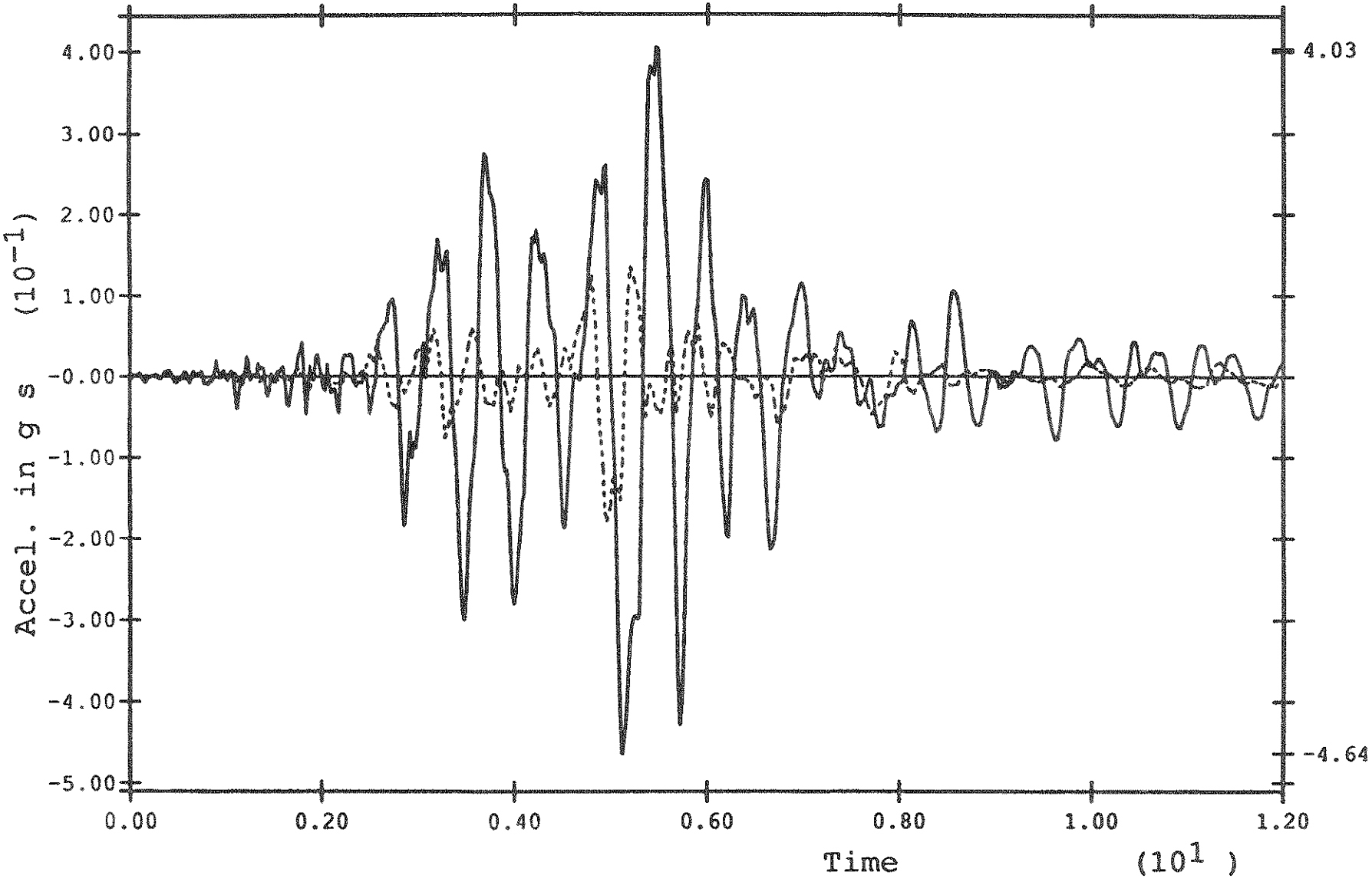

Fig.6-1 Measured Acceleration at Base(dashed) and Crest(solid),(up/downstream).

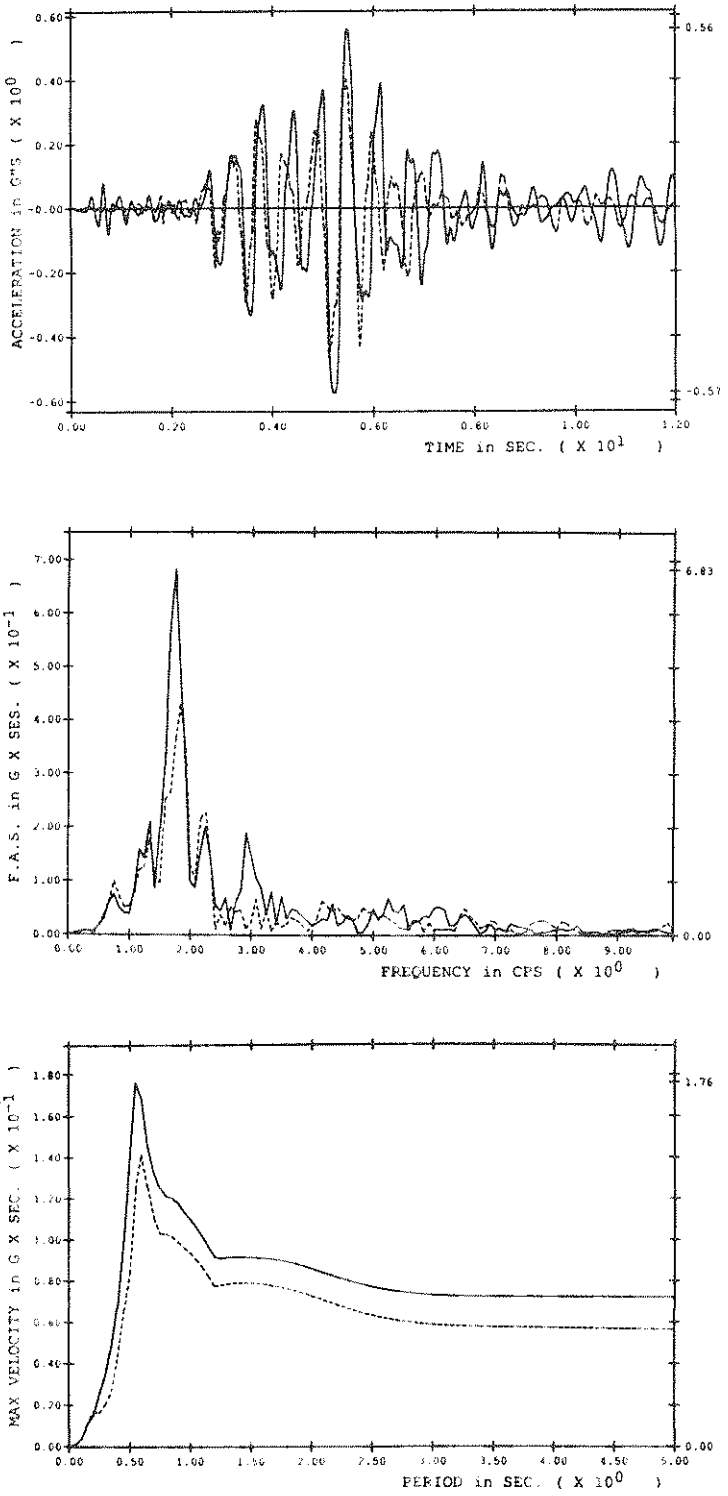

Fig.6-2 Computed Vs. Measured Motion at Station 20 (up/downstream,2-D). a)Acceleration b)FAS c)VRS.

$$s_{yy}^2 = \frac{1}{n}\sum_{i=1}^{n}(y_i - \bar{y})^2 \quad y - sample \;\; variance \tag{6.3}$$

$$s_{xy} = \frac{1}{n}\sum_{i=1}^{n}(x_i - \bar{x})(y_i - \bar{y}) \quad xy - sample \;\; covariance \tag{6.4}$$

with $\bar{x}$, $\bar{y}$ as the mean values.

Figure 6-3 gives the 'cumulative' correlation coefficient over field lengths increasing from 0 - 1 sec. to 0 - 12 sec. The correlation coefficient is always positive but quite variable over the first 6 secs. Over the full 12 secs. the correlation coefficient settled on a value just greater than 0.42.

A more interesting result is shown in Figure 6-4 where the effect of shifting one record relative to the other is observed. A shift of 1 sec. in each direction has been performed, and it is clear that an improvement in the correlation coefficient up to 0.72 can be achieved by shifting the origin of the computed values by - 0.08 secs.

The calculated acceleration in the vertical direction showed considerably less agreement with measured values. Part of the difficulty is explained by Figure 6-5 which shows superimposed plots of measured vertical acceleration at the base (dashed) and crest (solid) (stations 13 and 21 respectively). The excitation is considerably 'noisier' than in the up/downstream direction and less intense ie. the maximum recorded vertical acceleration at the crest is 0.185g compared with 0.403g in the up/downstream direction.

The computed accelerations in the vertical direction are compared with measured values in Figure 6-6a. The computed values (solid) show generally greater amplitudes than the measured values (dashed). The Fourier amplitude spectra of these time histories is given in Figure 6-6b and the measured values (dashed) indicate a broad band of frequencies with no particular frequency dominating the situation. The computed values (solid) also contain a broad bank of frequencies, but with clear peaks in the ranges 2-3 Hz and 5-6 Hz. The second eigenmode given in Figure 5-1b involved vertical motions and had a natural

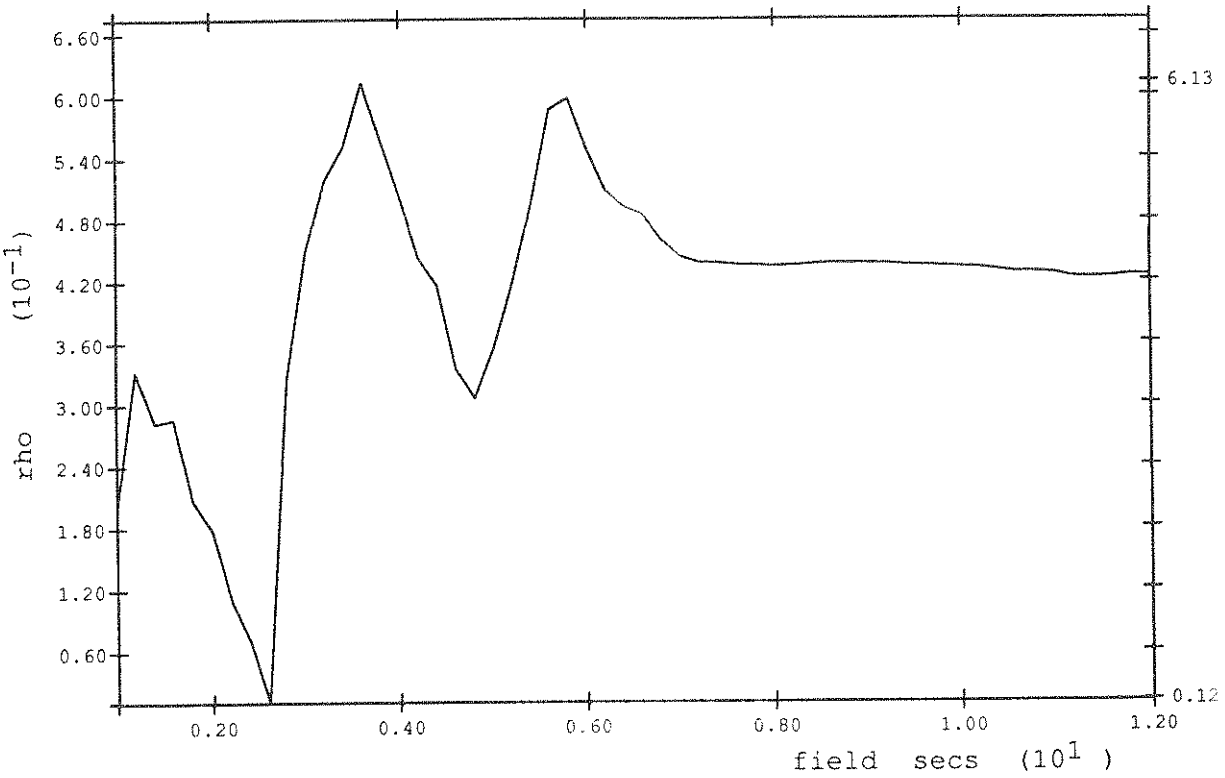

Fig. 6-3 Cumulative Correlation with Station 20(up/downstream, 2-D).

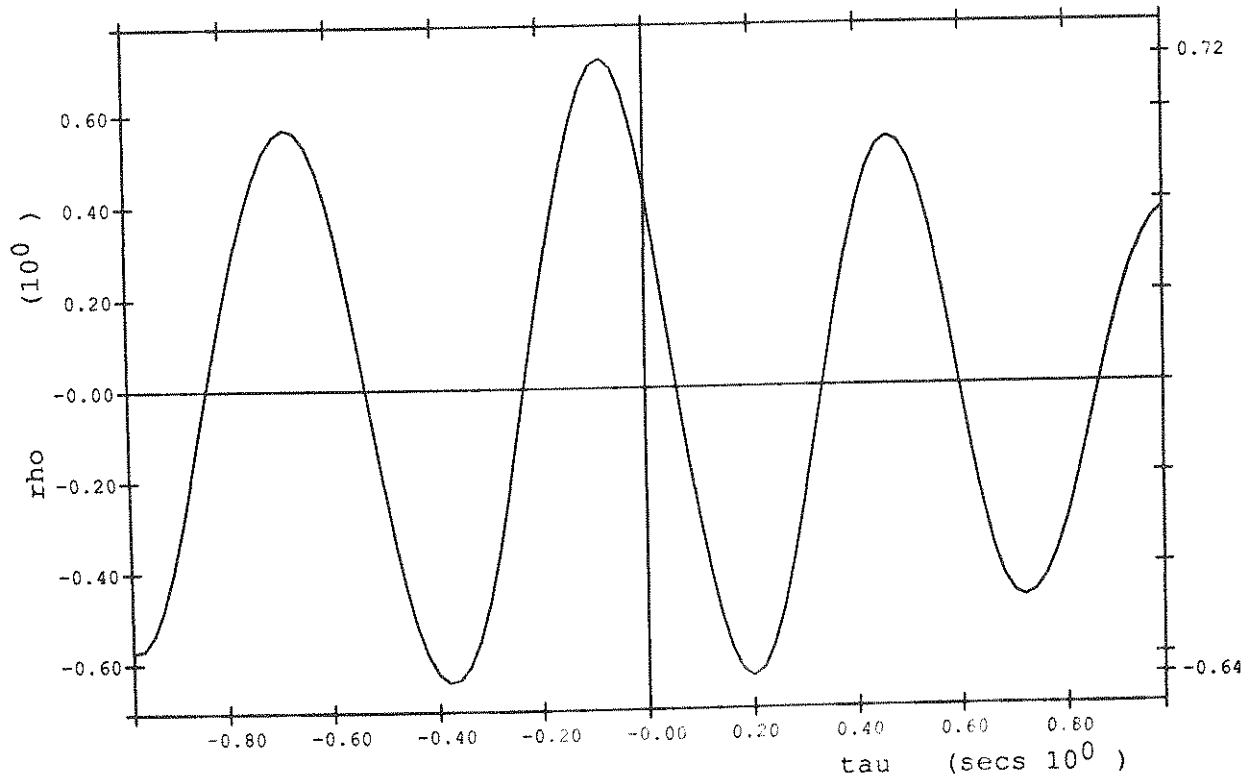

Fig. 6-4 Effects of Shifting on Correlation with Station 20(up/downstream,2-D).

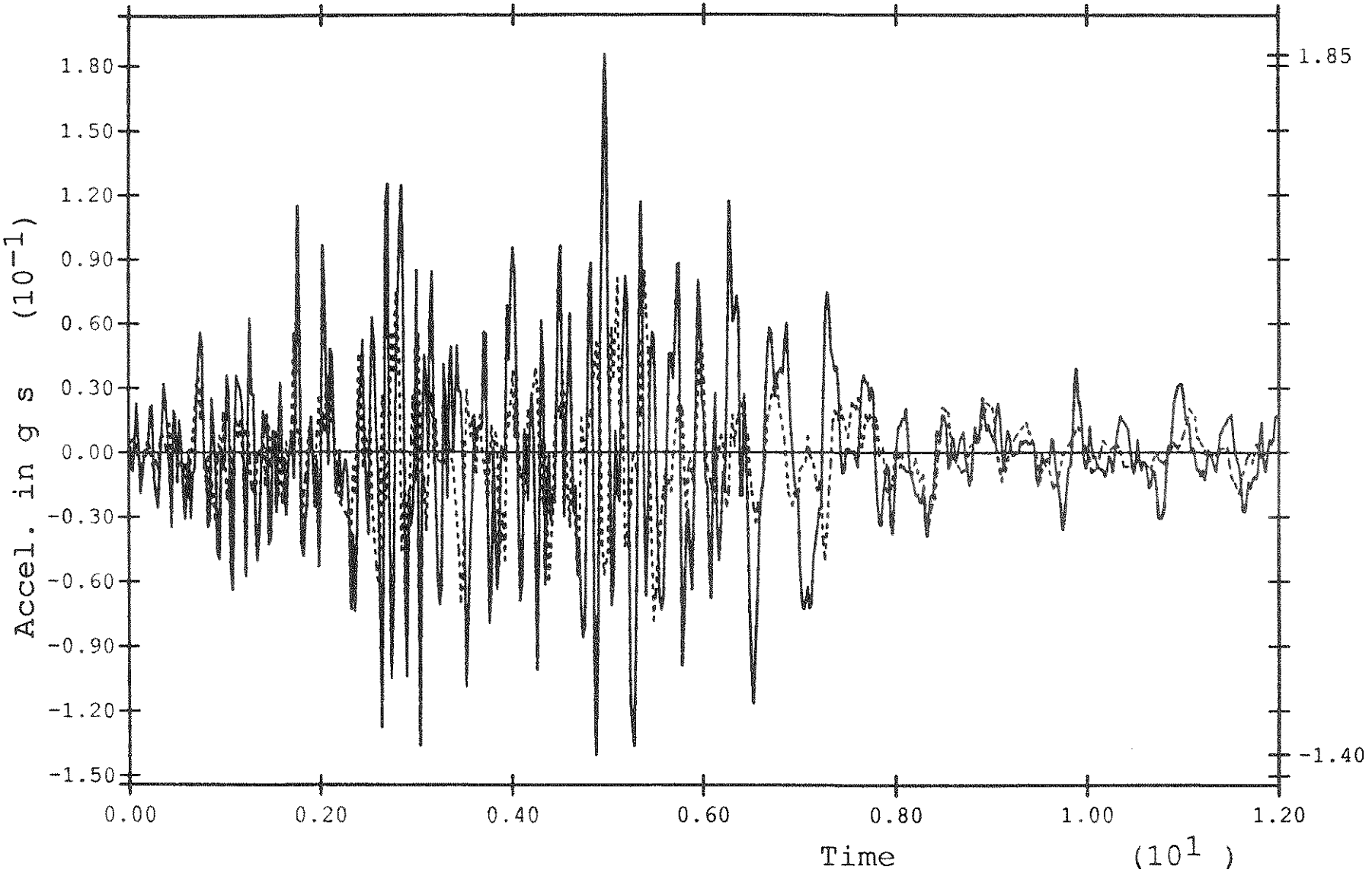

Fig.6-5 Measured Acceleration at Base(dashed) and Crest(solid),(vertical).

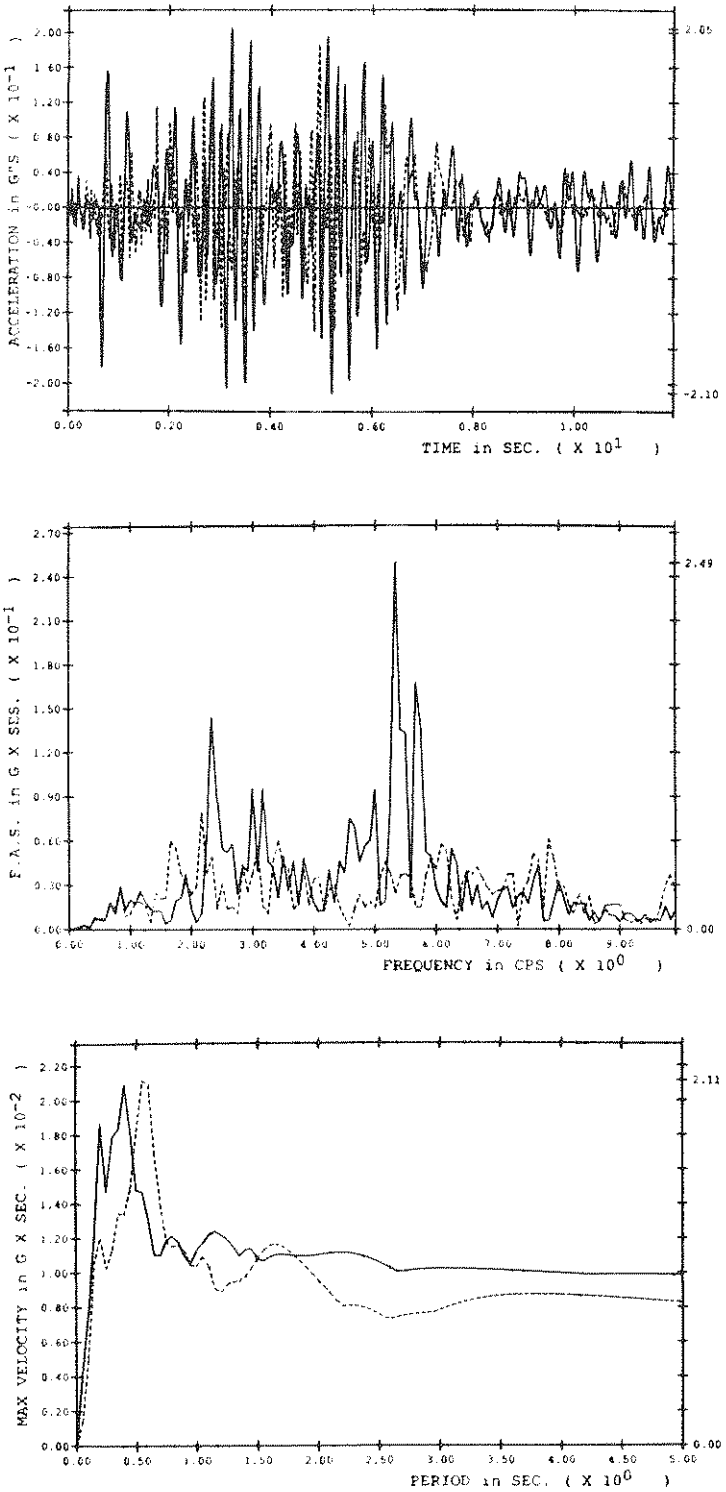

Fig.6-6 Computed vs. Measured Motion at Station 21 (vertical,2-D). a)Acceleration b)FAS c)VRS.

frequency of 2.15 Hz. The peaks of energy occurring in the 5-6 Hz range must correspond to higher eigenmodes. It should be noted, however, that the energy content in the vertical direction is considerably less than in the up/downstream direction, the peaks of the measured Fourier amplitude spectra being of the order 0.08g-sec and 0.43g-sec. respectively.

The velocity response spectrum for vertical motion (Figure 6-6c) gives velocities that are approximately an order of magnitude less than in the up/downstream direction. The shape of the two curves agrees quite well, however, with the measured values (dashed), showing a slightly higher natural period than the computed values (solid). The correlation between measured and computed vertical acceleration at the crest is rather poor as shown by Figures 6-7 and 6-8. In the cumulative case (Figure 6-7) the whole 12 sec record shows a very weak positive correlation of less than 0.1. Similarly, the effects of shifting (Figure 6-8) makes little improvement, and merely demonstrates the generally higher frequency content of the data.

6.2 Three dimensions

Using the same algorithm as in the 2-D case, the computed accelerations at three locations on the crest as shown in Figure 2-2 were compared with the measured values at stations 14 thru 16, 20 thru 22 and 4 thru 5. Figure 6-9a gives the computed and measured acceleration in the up/downstream direction at the crest centre line. As in the 2-D case, very good agreement is achieved, but due to the softer (logarithmic) stress/strain curve employed to generate the yield surfaces, the computed values give lower amplitudes than the measured values. The peak acceleration of 0.45g occurring between 5 and 6 secs. is well reproduced, however. It would appear that the computed amplitudes are quite sensitive to the shape of the stress strain curve between its initial gradient of G_o and its ultimate shear stress of q_{max}. The 'softer' the assumed stress/strain curve, the more hysteresis at low strain levels, and the greater the energy dissipation. This observation emphasizes the importance of

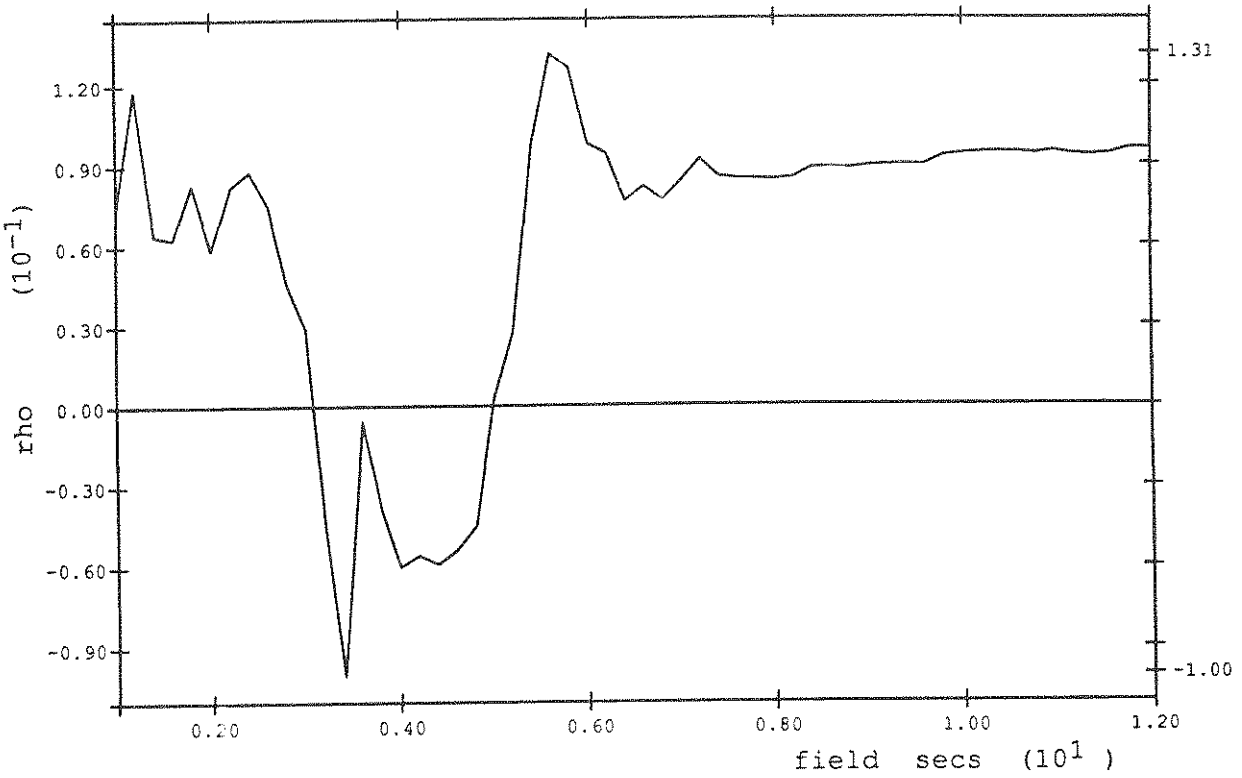

Fig. 6-7 Cumulative Correlation with Station 21 (vertical 2-D).

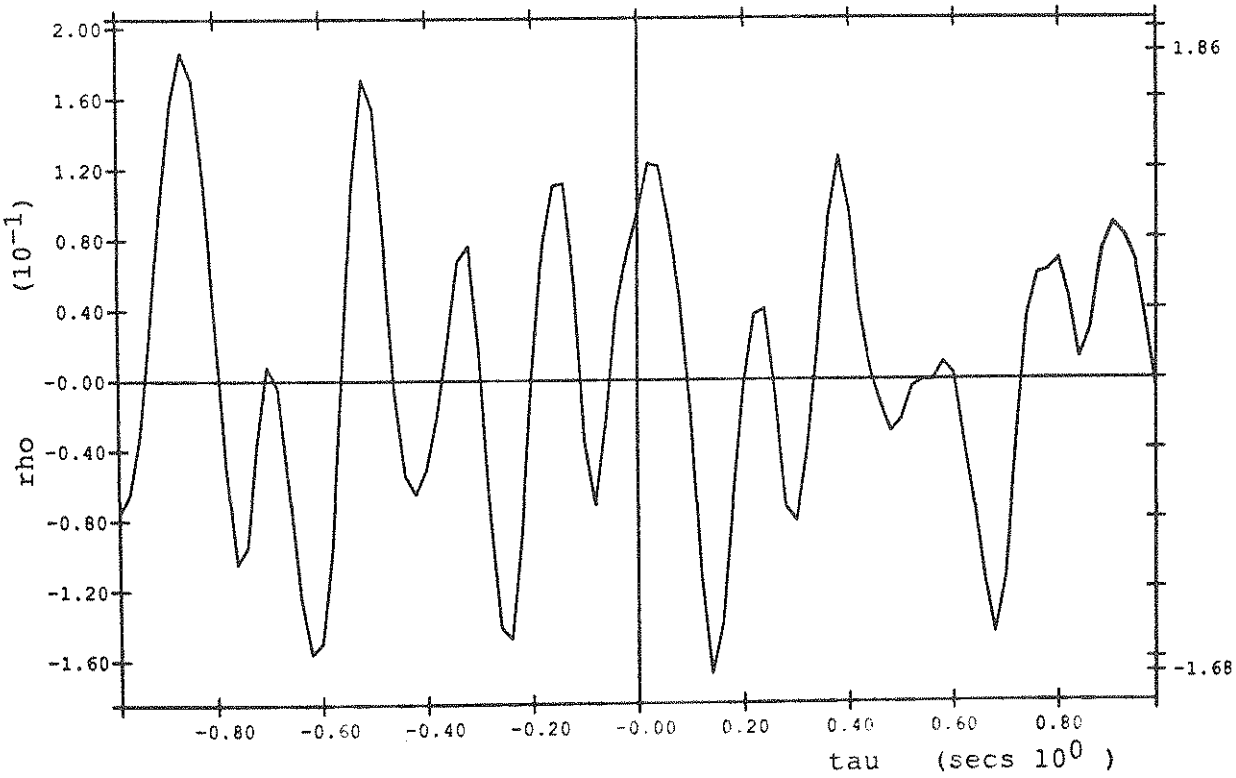

Fig. 6-8 Effects of Shifting on Correlation with Station 21(vertical, 2-D).

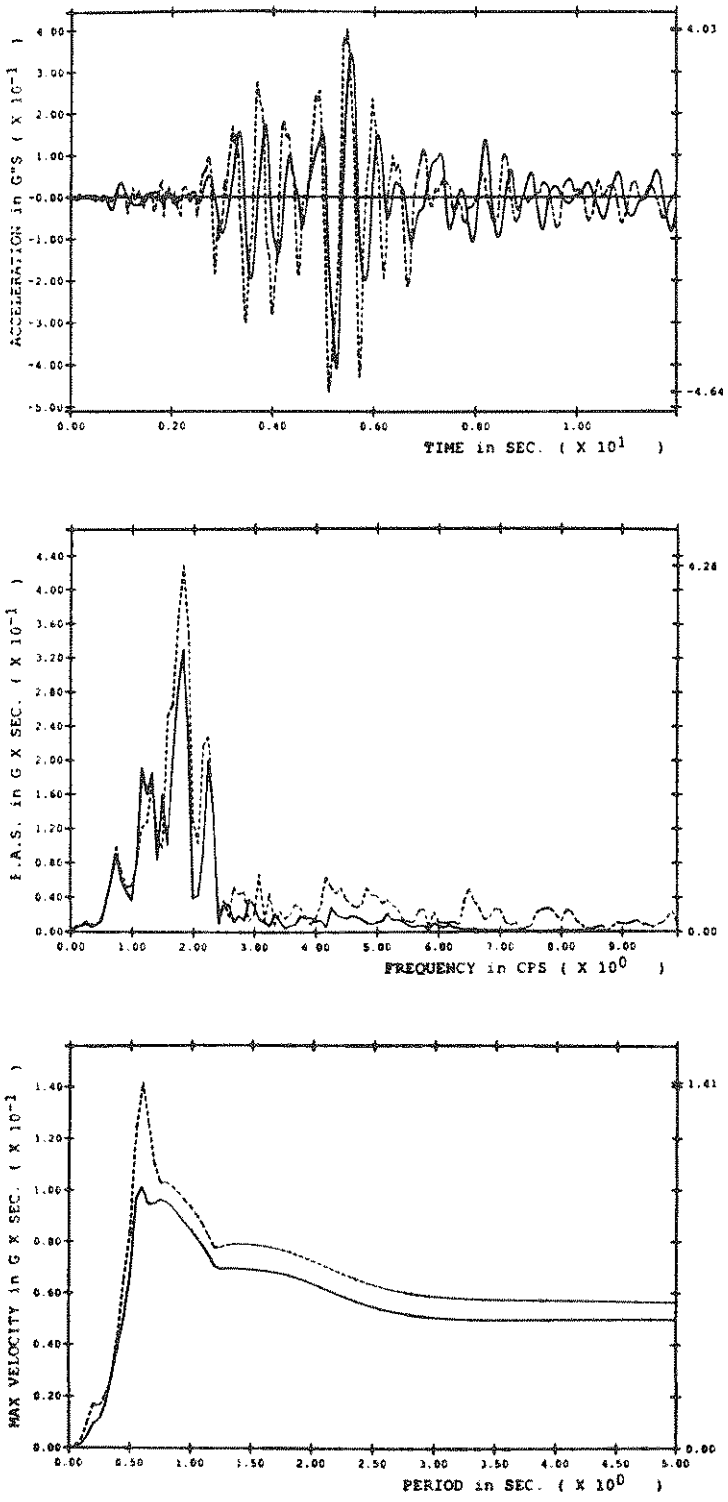

Fig.6-9 Computed vs. Measured Motion at Station 20 (up/downstream,3-D). a)Acceleration b)FAS c)VRS.

accurate modelling of the actual stress/strain curve obtained in laboratory tests.

The frequency content of the up/downstream motion are compared in Figure 6-9b and 6-9c in the form of Fourier and velocity response spectra. These show that the energy is concentrated at a frequency of just under 2Hz . The correlation coefficient shown in Figure 6-10 for the full 12 sec time history converges on a value around 0.5. The effects of shifting shown in Figure 6-11 indicate that a maximum correlation of 0.86 could be achieved. These results represent a small improvement over the 2-D counterparts.

The computed results in the vertical (y-) and transverse (z-) direction at the crest centerline gave little or no correlation with measured values. The vertical response shown in Figure 6-12a indicates computed values with substantially lower amplitudes than the measured values. The frequency content of the vertical acceleration in the form of Fourier and velocity response spectra (Figures 6-12b and 6-12c) indicates that the computed values have been unable to reproduce the higher frequencies present in the broad band of measured frequencies. Similar remarks can be made with regard to the computed transverse acceleration given in Figures 6-13.

The computed values of acceleration obtained at other locations on the crest (Figure 2-2) fell into a similar pattern. The up/downstream values were generally quite good, but the other direction dissapointing. Figure 6-14a shows the computed (solid) values at node 383 compared with the measured (dashed) values at station 4. The amplitudes are lower than at the centreline as would be expected as the rigid valley wall is approached. The Fourier and velocity response spectra are given in Figures 6-14b and 6-14c and show that the frequency content is quite well reproduced. The correlation coefficient for the full 12 sec time history converges on a value of around 0.43 (Figure 6-15) whereas the effects of shifting (Figure 6-16) indicate that a correlation as high as 0.68 could be achieved.

The vertical accelerations computed at node 383 (solid) are compared with the measured

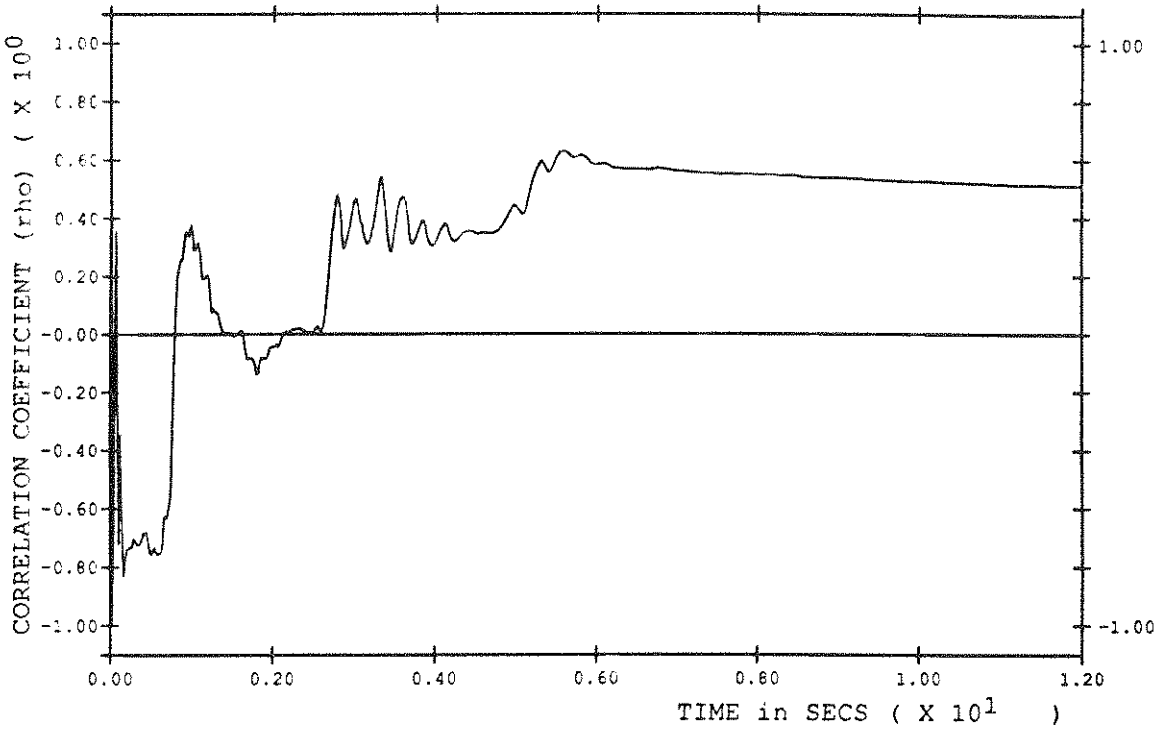

Fig.6-10 Cumulative Correlation with Station 20 (up/downstream,3-D).

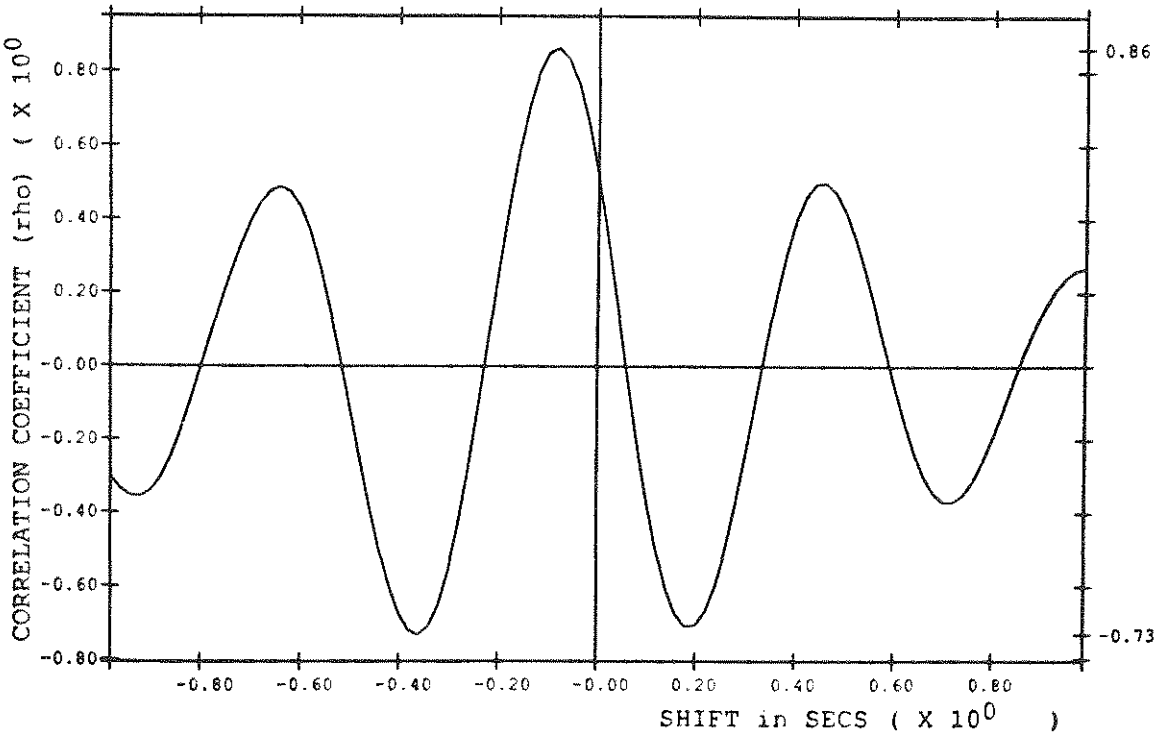

Fig.6-11 Effects of Shifting on Correlation with Station 20 (up/downstream,3-D).

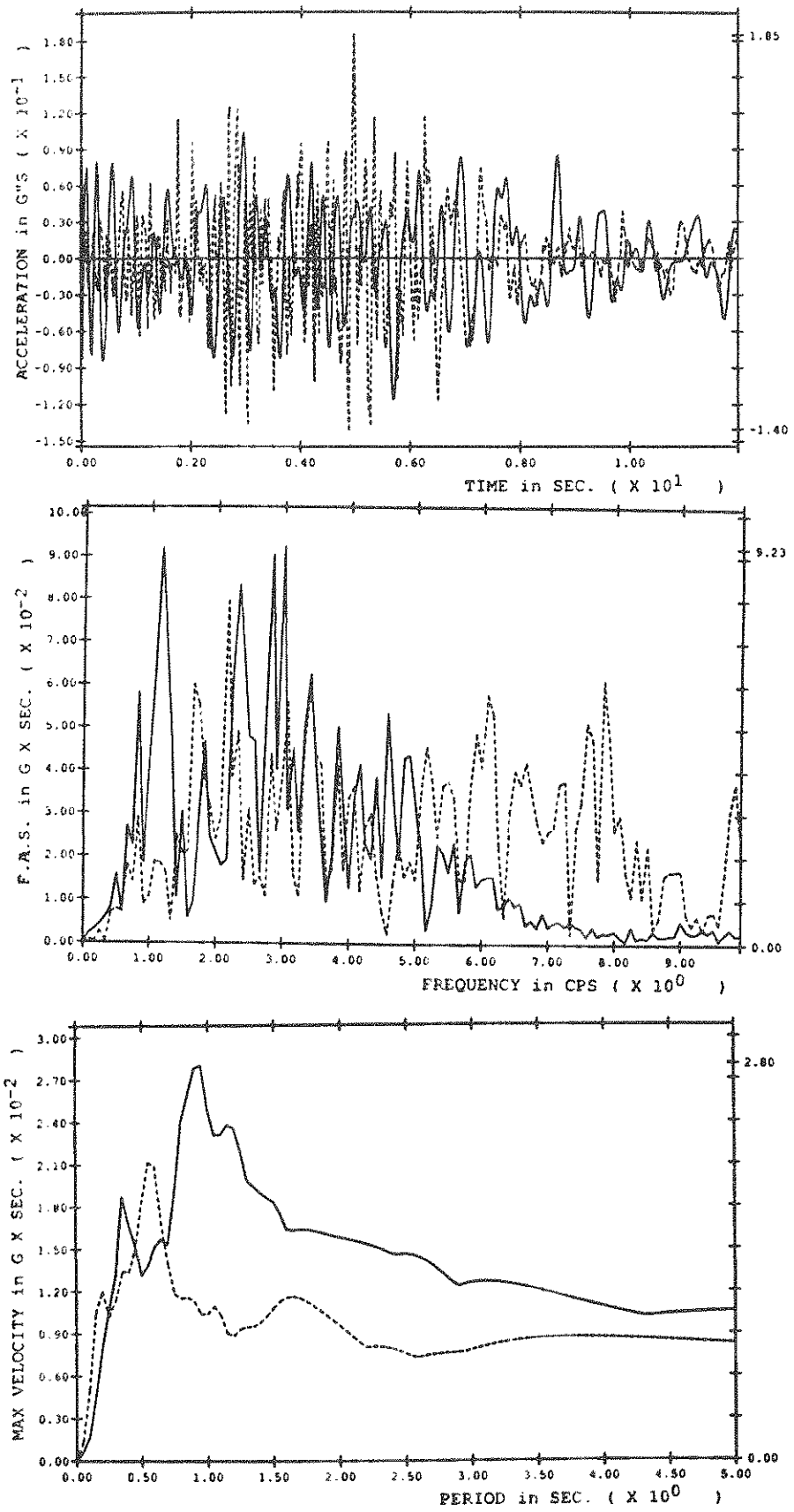

Fig.6-12 Computed vs. Measured Motion at Station 21 (vertical,3-D). a)Acceleration b)FAS c)VRS.

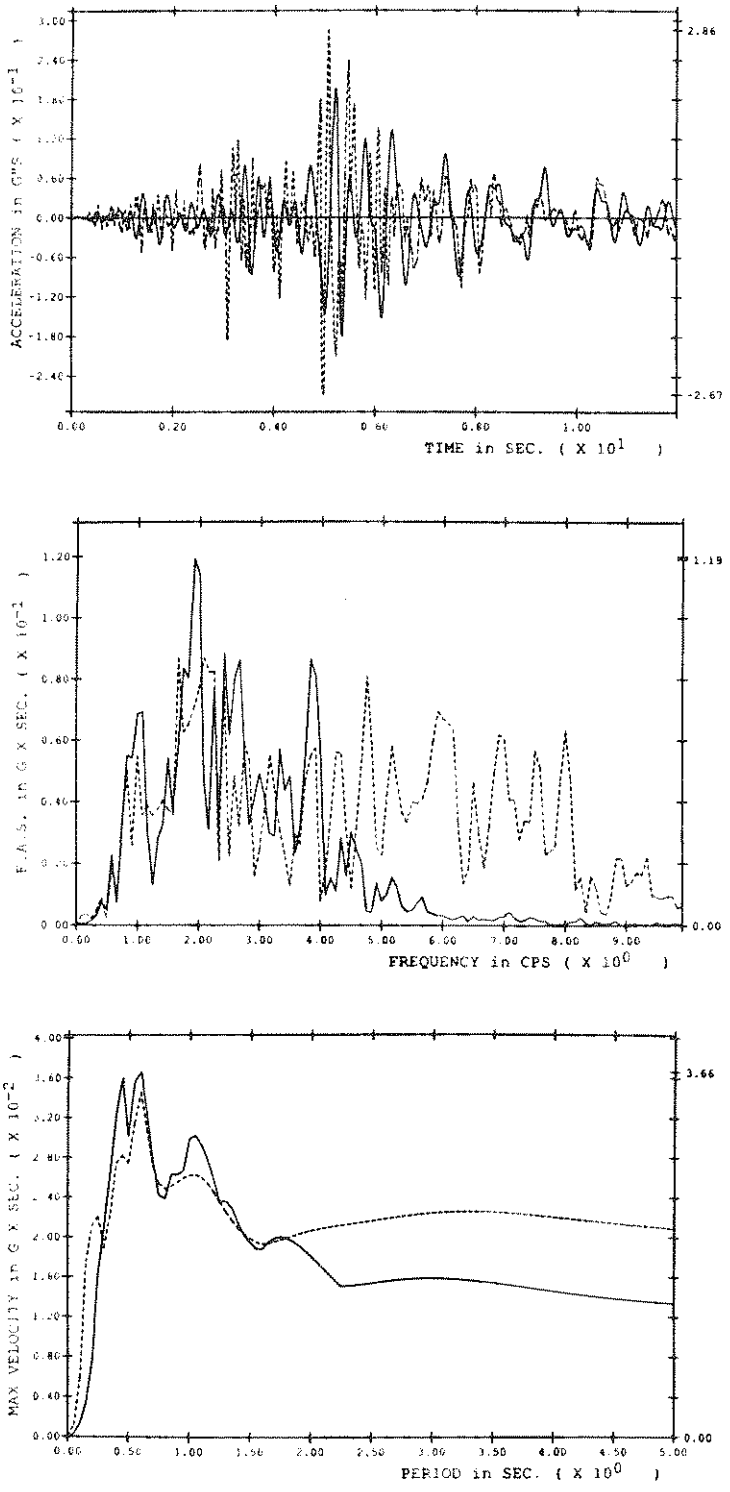

Fig.6-13 Computed vs. Measured Motion at Station 22 (transverse,3-D). a)Acceleration b)FAS c)VRS.

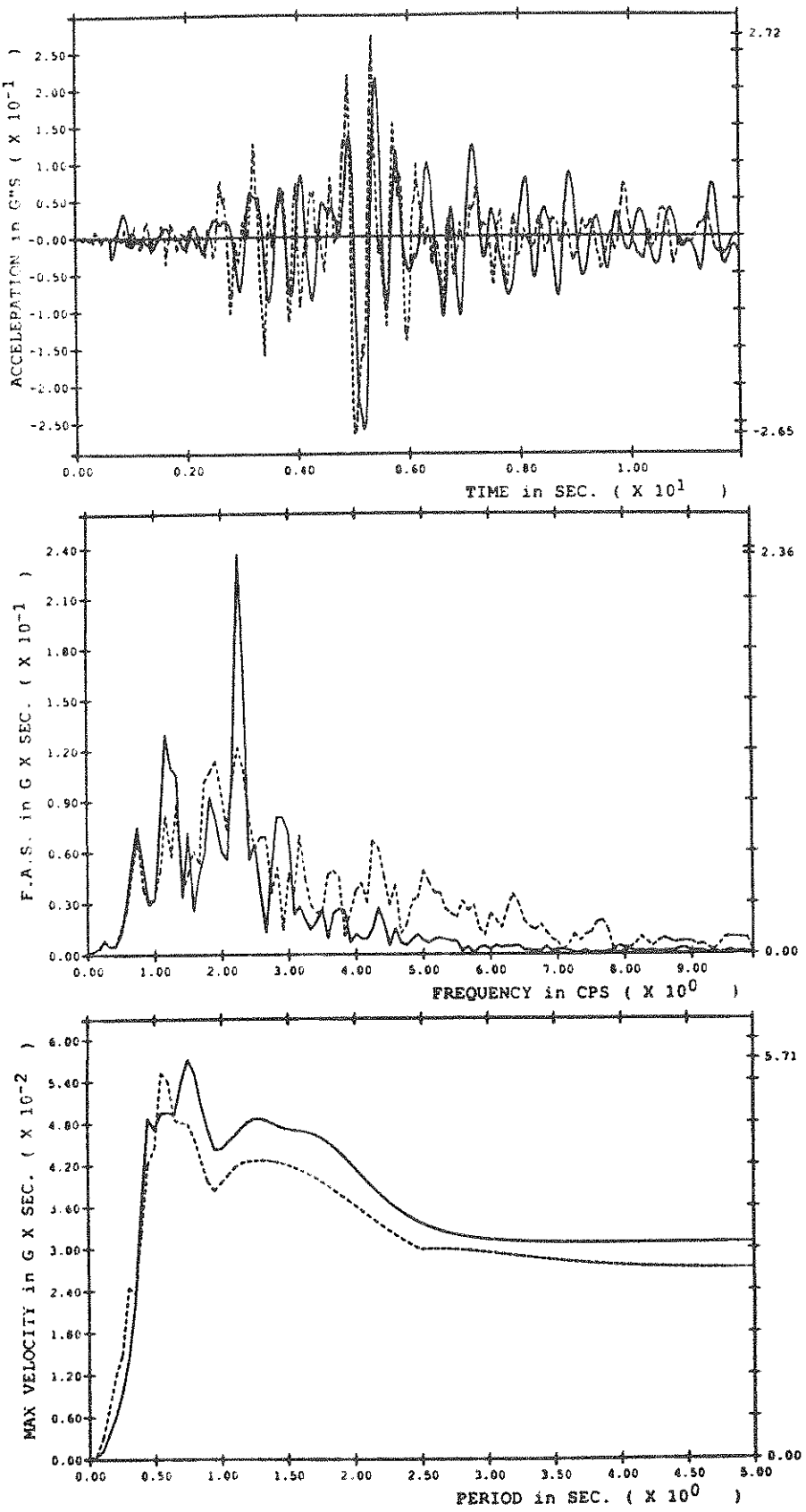

Fig.6-14 Computed vs. Measured Motion at Station 4 (up/downstream,3-D). a)Acceleration b)FAS c)VRS

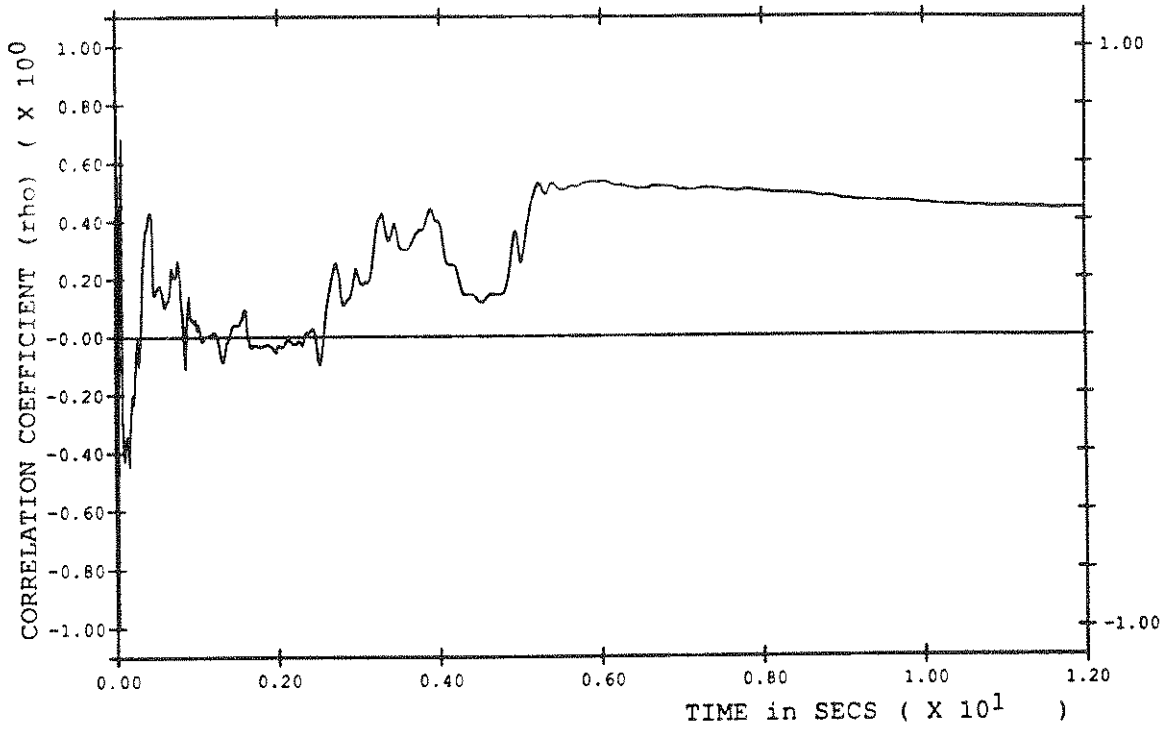

Fig.6-15 Cumulative Correlation with Station 4(up/downstream,3-D)

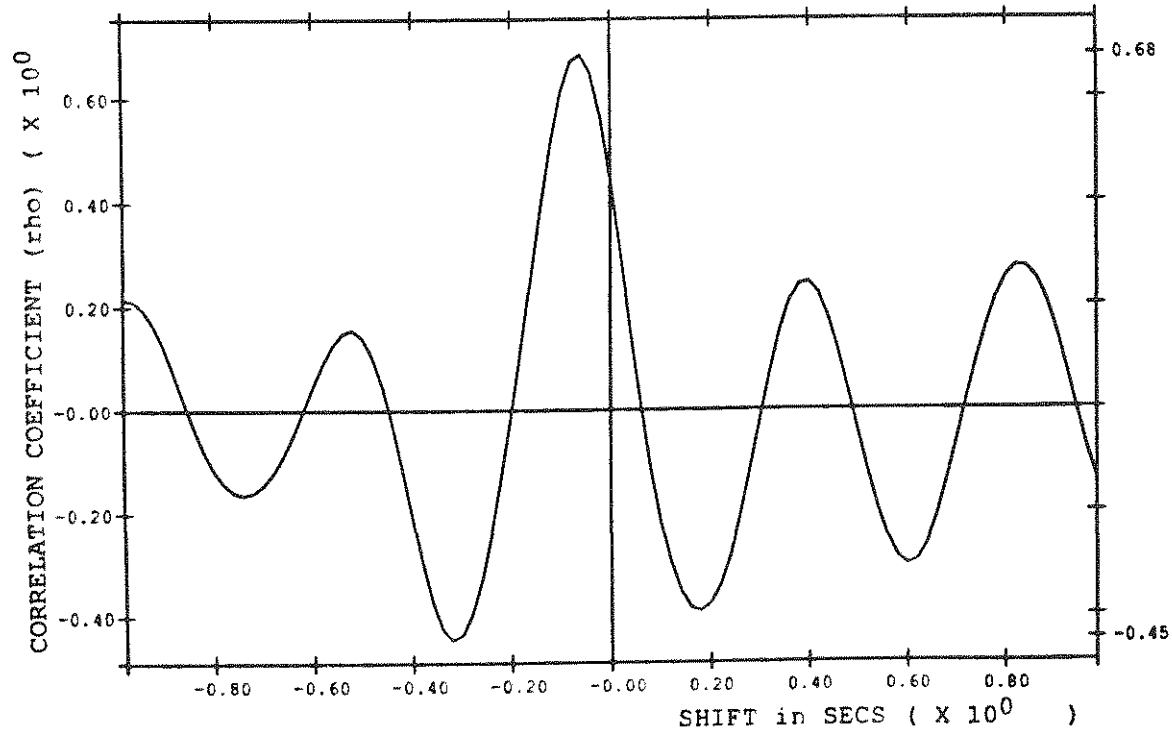

Fig.6-16 Effects of Shifting on Correlation with Station 4(up/downstream,3-D)

values at station 5 (dashed) in Figure 6-17a and show poor agreement in the frequency content. The amplitude levels are in general agreement however. The Fourier spectrum for these results given in Figure 6-17b confirm that the measured values (dashed) contain more high frequencies that could be captured by the finite element analysis. No measured values were available in the transverse (z-) direction at this location.

Corresponding to the other side of the crest, computed results at node 777 (Figure 2-2) were also compared with measured values at stations 14, 15 and 16. In the up/downstream direction (Figure 6-18), the computed values underestimated the peak acceleration measured at station 14 but the frequencies were reasonably well reproduced as shown by the Fourier and velocity response spectra (Figures 6-18b anc 6-18c). The correlation coefficient for the full 12 sec time history was about 0.43 whereas shifting of the data could improve this value to 0.56 (Figures 6-19 and 6-20).

Comparisons of computed values at node 777 with measured values at stations 15 and 16 in both time and frequency domains are shown in Figures 6-21 and 6-22. These follow the same pattern as the previous comparisons, in that the high frequencies of the measured values were not reproduced by the finite element analysis. Although the amplitude levels were of generally similar order, the acceleration measured (dashed) at 5 secs in both Figures 6-21a and 6-22a was underestimated by the computed values. It would appear that a stiffer stress/strain curve might increase the computed amplitudes, but possibly at the expense of inadequate hysteretic damping.

It is also possible that the inability of the model to reproduce the higher frequencies is caused partly by the relatively crude finite element discretisation used in the 3-D analysis. To address this possibility, a finer 3-D mesh has been prepared for further analyses of the Long Valley Dam. The mesh, shown in skeletal form in Figure 6-23, uses the 2-D mesh of Figure 2-1 as a parent section and contains a total of 17 sections in the transverse direction.

The mesh has 2121 nodes and 1494 elements distributed between 9 element groups. The size of the mesh will require runs to be made on Princeton's CYBER 205 'supercomputer' and the results will be presented in a subsequent report.

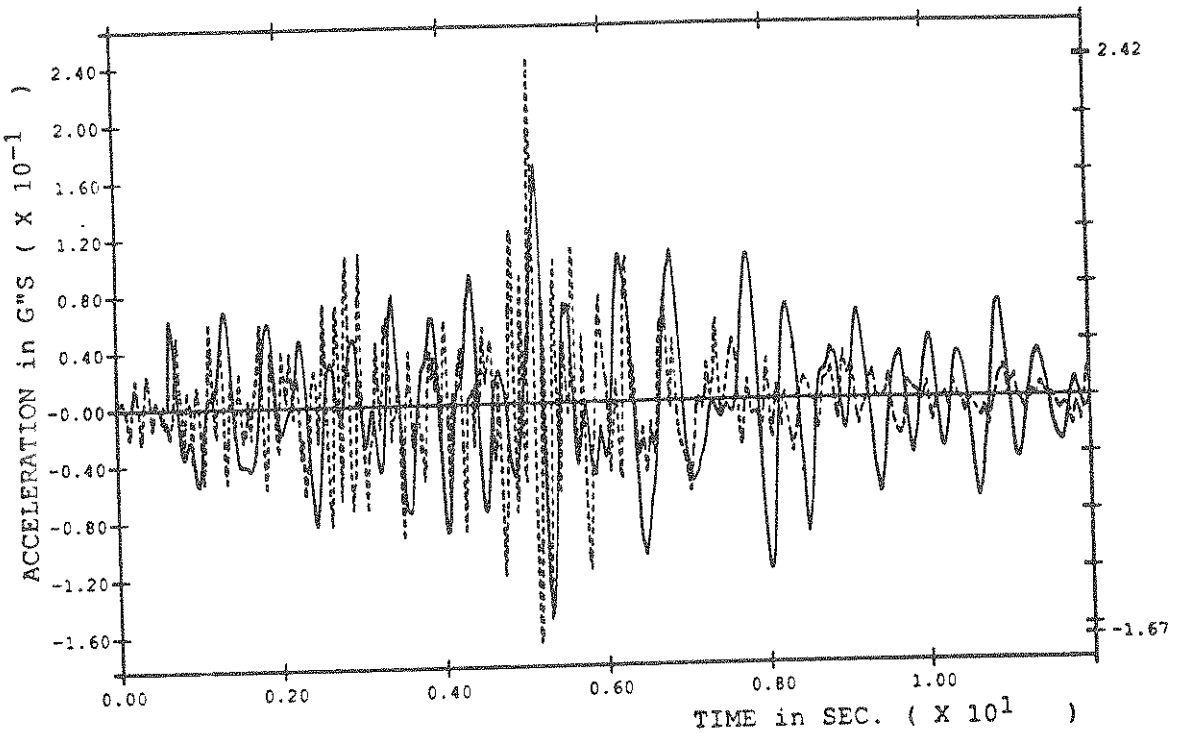

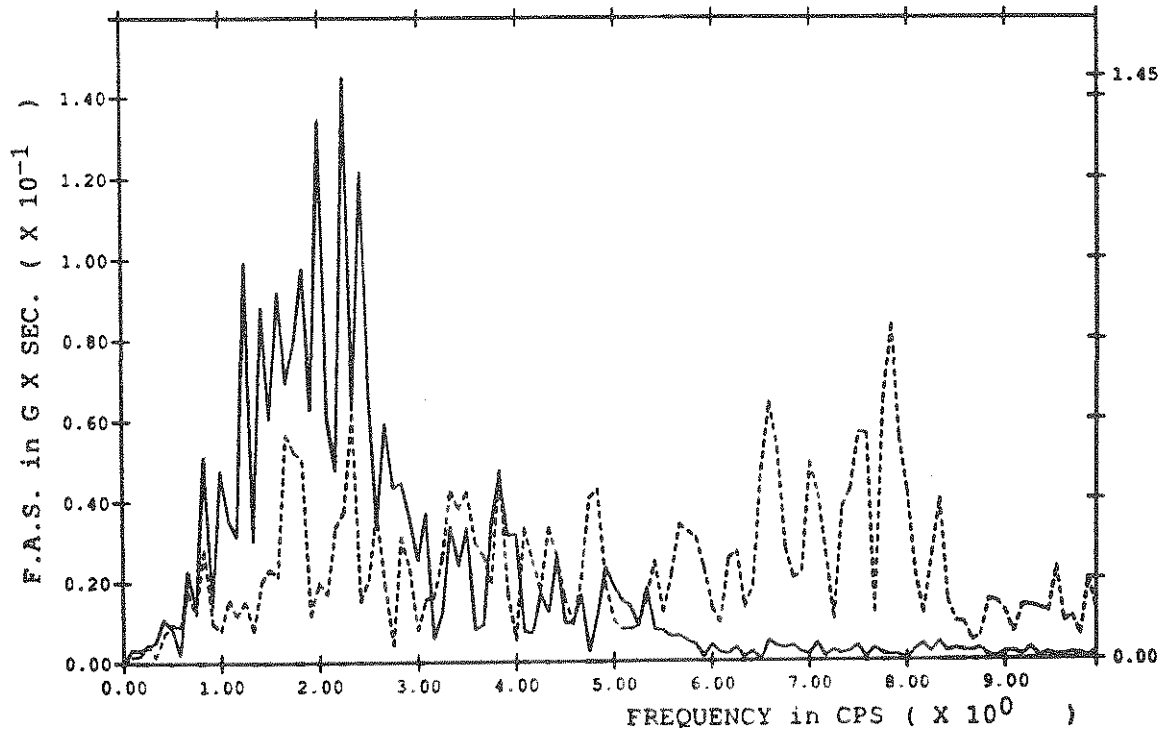

Fig.6-17 Computed vs. Measured Motion at Station 5 (vertical,3-D).
a)Acceleration b)FAS

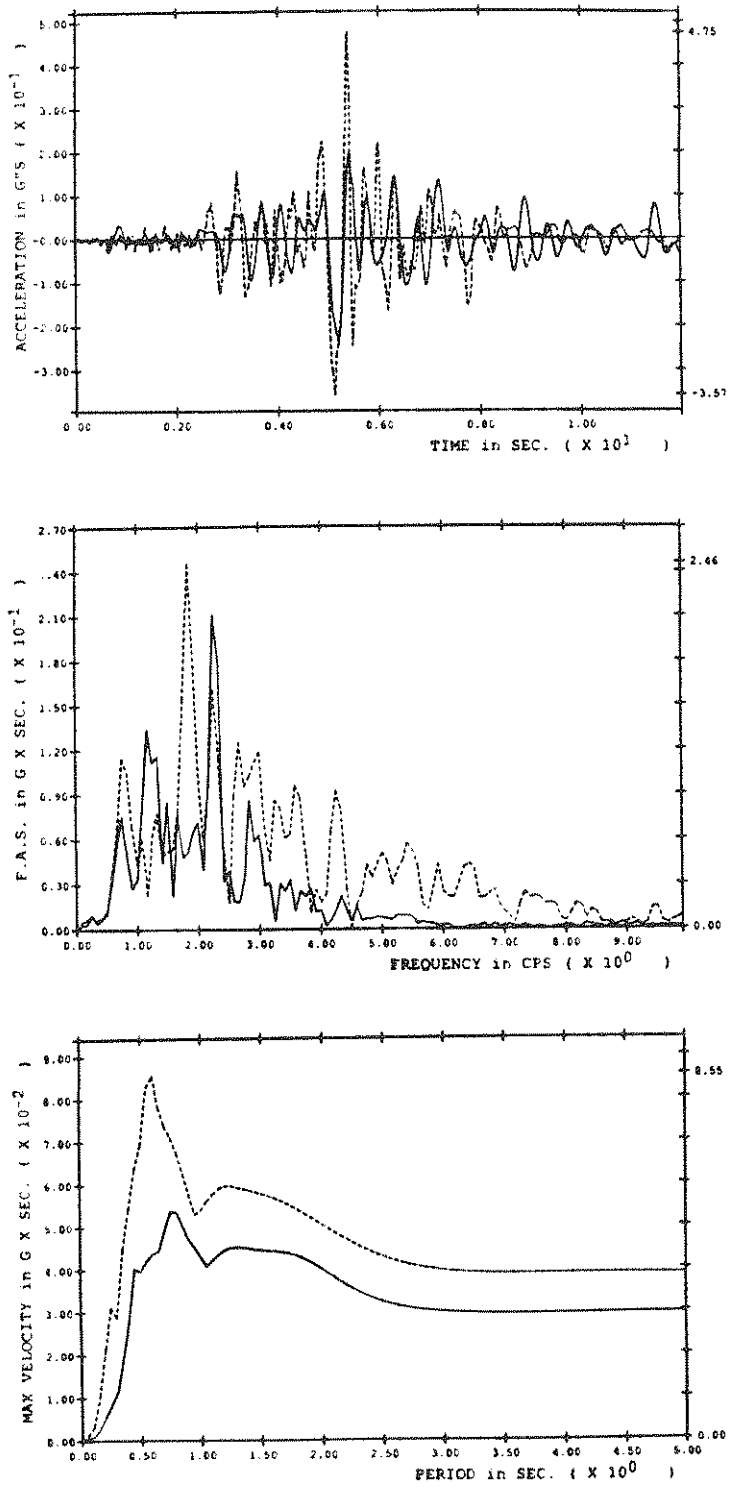

Fig.6-18 Computed vs. Measured Motion at Station 14 (up/downstream,3-D). a)Acceleration b)FAS c)VRS.

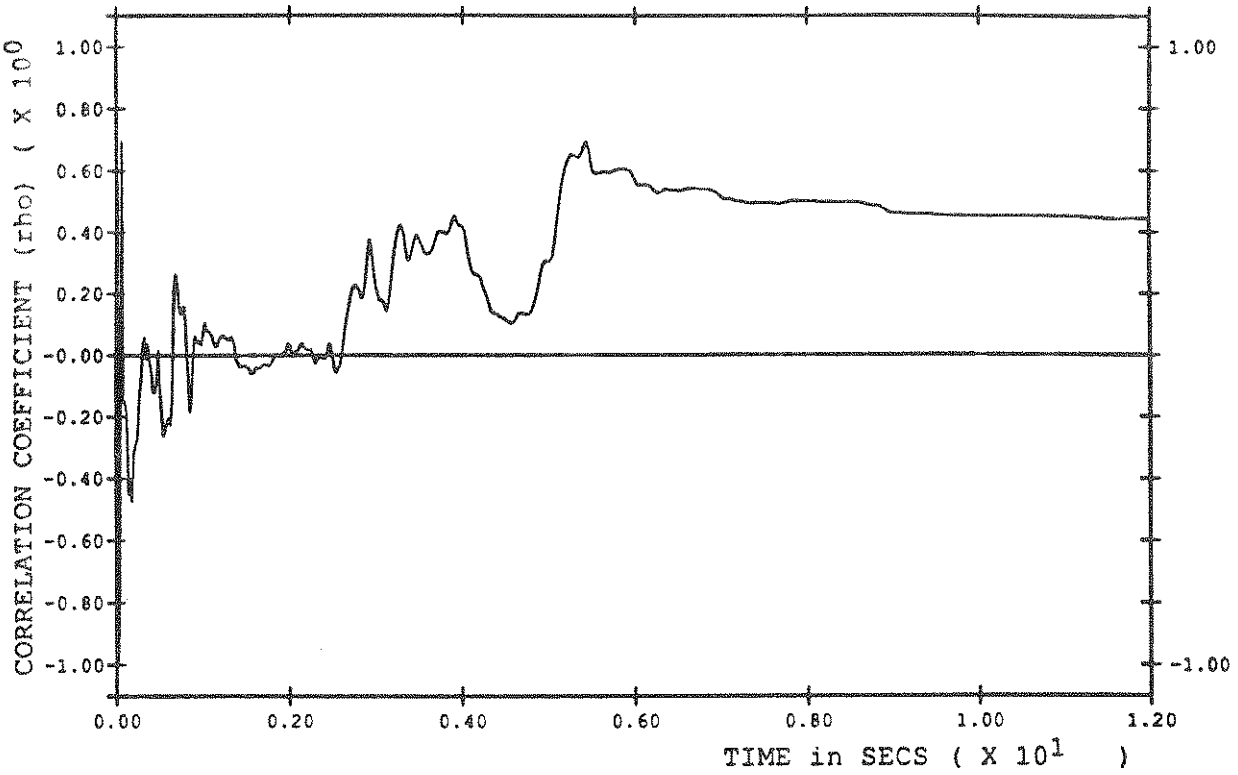

Fig.6-19 Cumulative Correlation with Station 14(up/downstream,3-D).

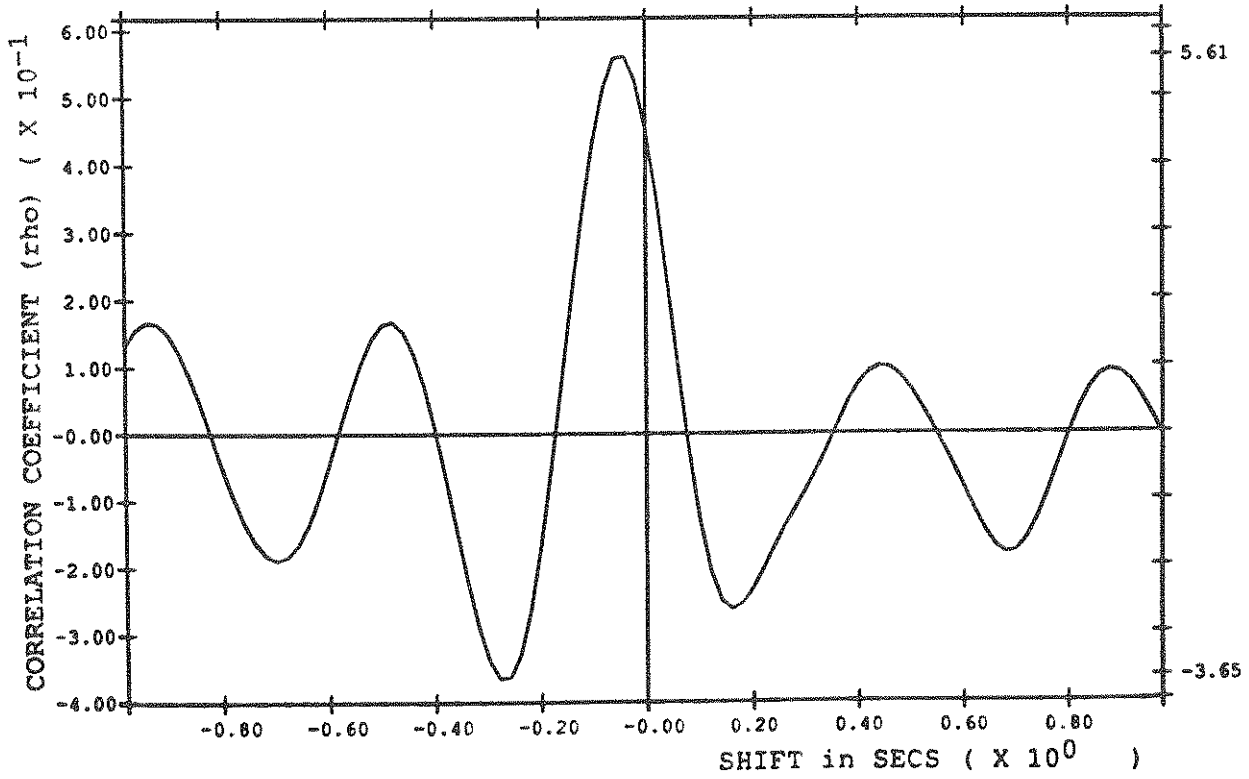

Fig.6-20 Effects of Shifting on Correlation with Station 14 (up/downstream,3-D).

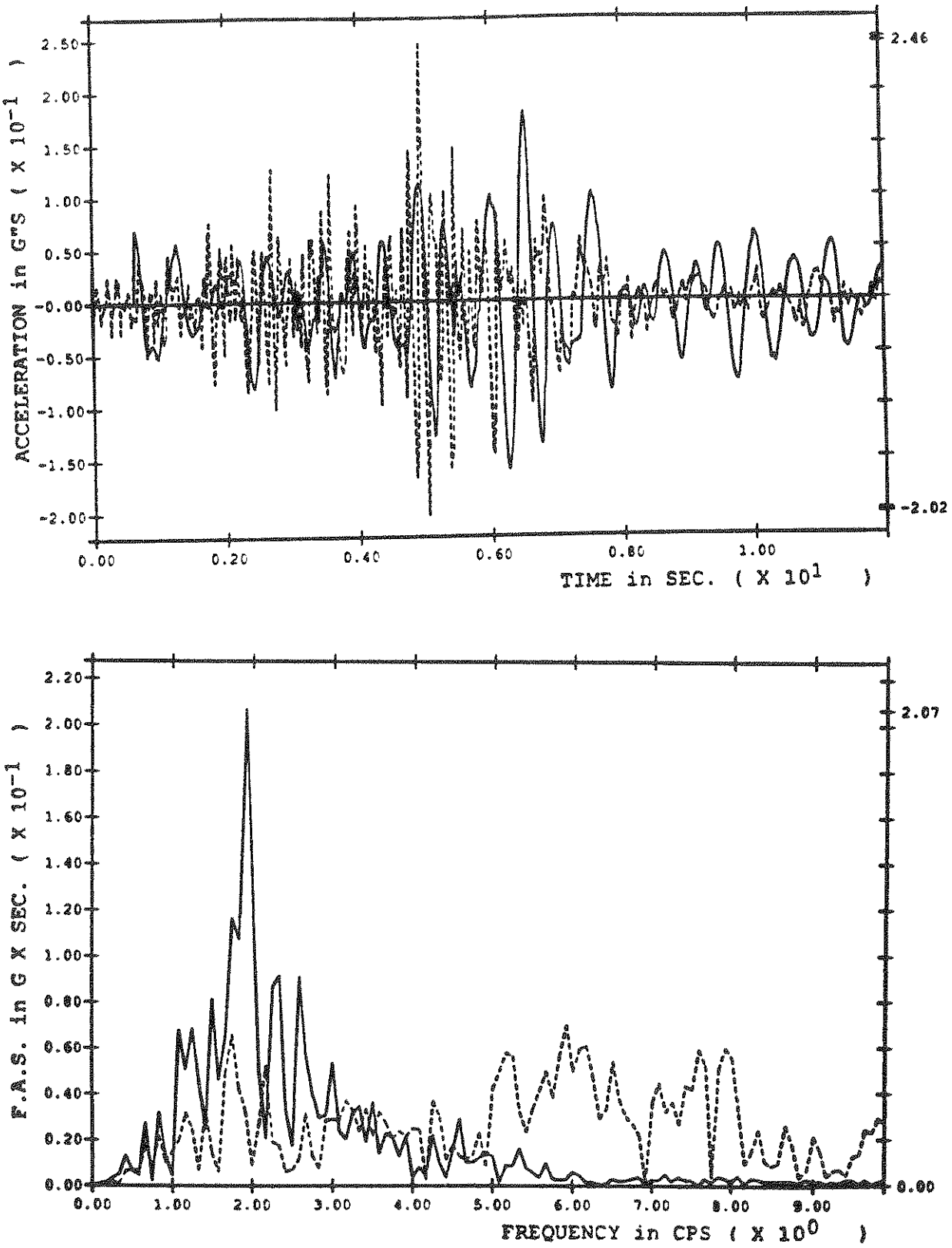

Fig.6-21 Computed vs. Measured Motion at Station 15 (vertical,3-D).
a) Acceleration b)FAS

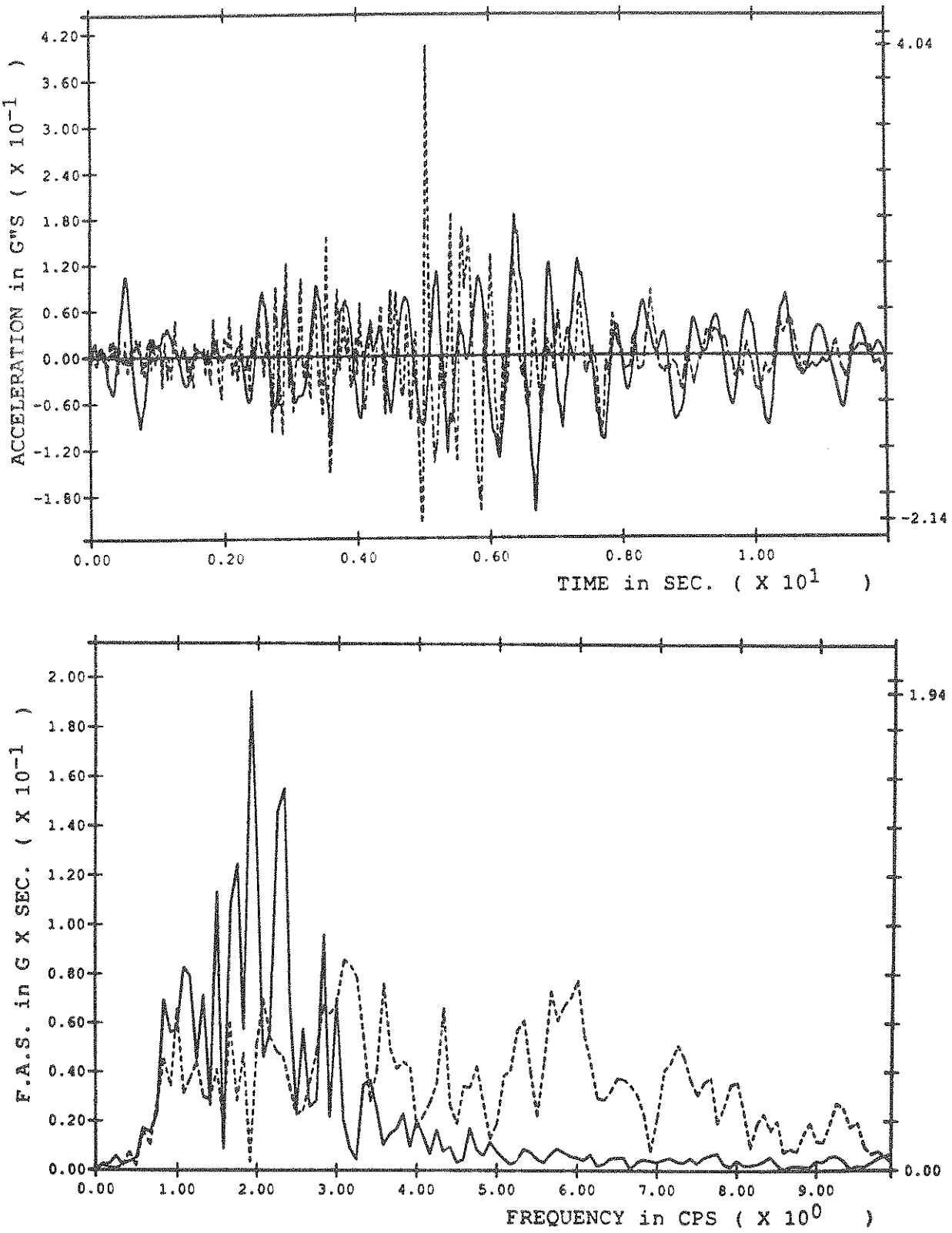

Fig.6-22 Computed vs. Measured Motion at Station 15 (transverse,3-D).
a)Acceleration b)FAS

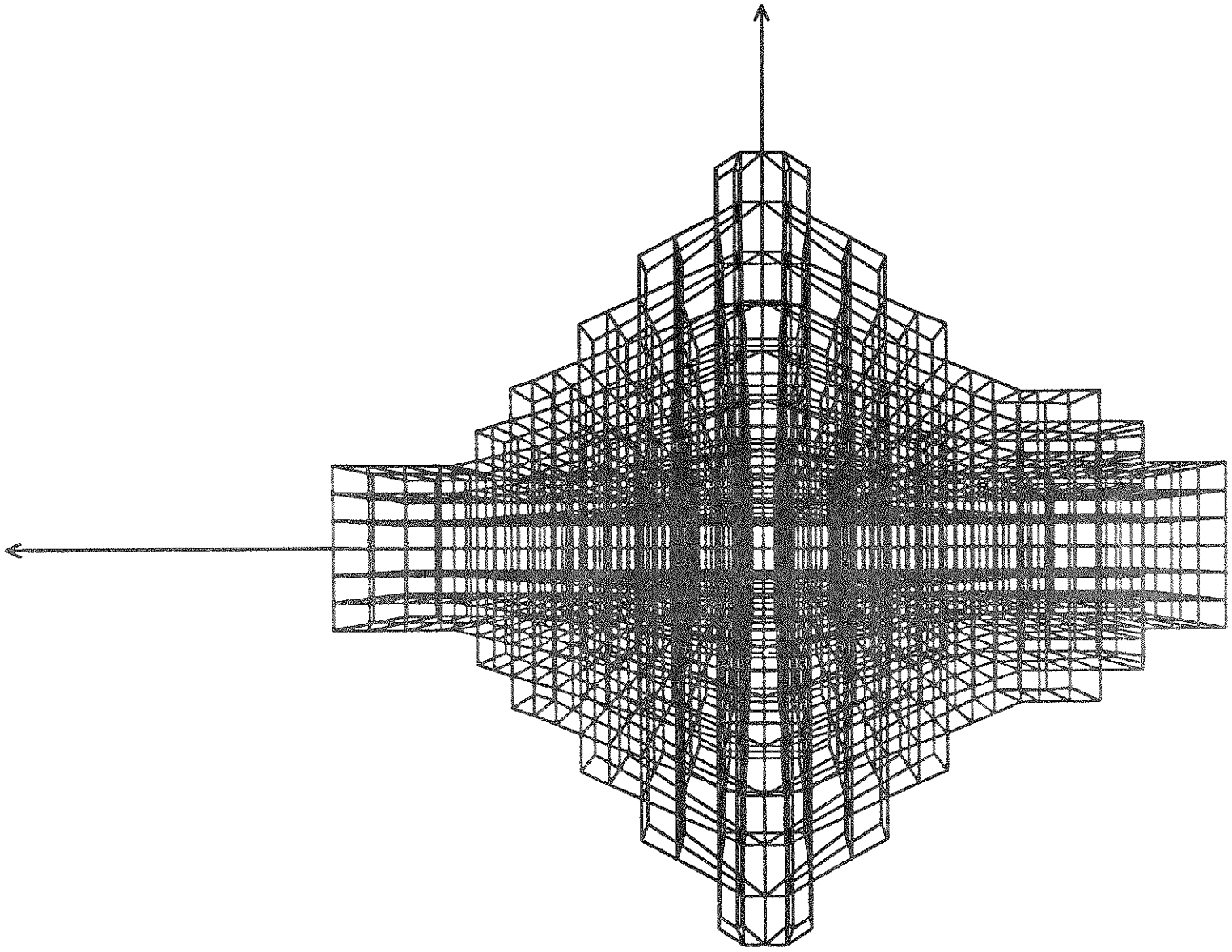

Fig.6-23 Skeletal Plan View of Refined 3-D Mesh

SECTION 7

CONCLUSIONS

The report has presented results comparing the measured and computed behavior of the Long Valley Dam subjected to earthquake excitation. Both 2-D and 3-D analyses were performed, and results obtained for the natural frequencies and acceleration time histories of the crest of the dam. The computed values were compared with natural frequencies estimated by spectral analyses, and time histories measured by a number of accelerographs placed on the dam. Both analyses gave reasonably close agreement with the natural frequencies of the dam, but the 3-D case performed slightly better. Care must be exercised, however, when comparing natural frequencies, to ensure that the same mode of vibration is being considered in each case. The finite element frequencies tended to overestimate the measured natural frequencies of the dam due to non-linear effects in the actual structure resulting in degraded stiffness.

A consistent pattern emerged in the acceleration time histories computed at the crest. In both the 2-D and 3-D analyses, encouraging agreement was obtained between computed and measured values in the up/downstream direction. This was true for both amplitude levels and frequency content. The 3-D results gave marginally better agreement than the 2-D case and showed a potential correlation coefficient of 0.86.

The computed values in the y-direction in the 2-D analysis, and the y- and z-directions in the 3-D analysis did not, however, give good agreement. The amplitude levels were of the correct order, but the computed values failed to reproduce the high frequencies present in the measured crest acceleration. This was particularly true in the 3-D analysis. It is suggested that better results might be obtained if a stiffer stress/strain curve was used to model the transition from the initial gradient to peak shear stress q_{max}. This might have an adverse effect on the more important up/downstream results, however, and the reduced hys-

teretic damping might result in the response failing to attenuate in time.

A further consideration is the ability of the finite element discretisation itself to capture the higher frequencies. In order to further examine this possibility, a considerably finer 3-D mesh is presently being prepared for further analyses.

SECTION 8

LIST OF NOTATIONS

ν_o , G_o , E_o	Initial elastic parameters.
c' , ϕ'	Effective shear strength parameters.
K_o , K_p	At rest, and passive earth pressure coefficients.
p	$(\sigma_1 + \sigma_2 + \sigma_3)/3$ mean stress.
q	$(\sigma_1 - \sigma_3)$ shear stress.
p_o , q_o	Initial values.
q_{max}	Peak value.
dp / dq	Gradient of p vs. q.
$\overline{\varepsilon}$	$(\varepsilon_1 - \varepsilon_3)$ shear strain.
A , B	Curve fitting parameters.
α , β	Time stepping parameters.
$\overline{x}$, $\overline{y}$	Mean values.
r_{xy}	Correlation coefficient between x and y.
s_{xx}^2	x-sample variance.
s_{xy}^2	y-sample variance.
s_{xy}	x-y covariance.
n	Number of records.
Δt	Time step.
τ	Time shift.

SECTION 9

REFERENCES

1. J-H. Prevost "Mathematical Modeling of Monotonic and Cyclic Undrained Clay Behavior", IJNAMG, Vol. 1, No. 2, 1977, pp. 195-216.

2. S.J. Lacy and J-H. Prevost "Nonlinear seismic response analysis of earth dams", Soil Dynamics and Earthquake Engineering, vol.6, No.1, 1987, pp.48-63.

3. W.W. Hoye, J.L. Hegenbart and S. Matsuda "Long Valley Dam stability evaluations" City of Los Angeles Dept. of Water and Power, Report No. AX 203-24, 1982.

4. C.D. Turpen "Strong motion records from the Mammoth Lakes earthquakes of May 1980" CDMG Preliminary Report, 27, 1980, p.42.

5 S.S. Lai and H.B. Seed "Dynamic response of Long Valley Dam in the Mammoth Lake earthquake series of May 25-27 1980" Earthquake Engineering Research Center Report No. UCB/EERC-85/12, November 1985.

6 J.H. Prevost "DYNAFLOW: A nonlinear transient finite element program" Report 81-SM-1, Civil Engineering Department, Princeton University, Princeton, N.J. 08544, January 1981. Most recent revision September 1987.

7. J-H. Prevost, A.M. Abdel-Ghaffar and S.J. Lacy "Non Linear Dynamic Analysis of an Earth Dam". J. Geotech. Eng. Div., ASCE, Vol. 111, No. 7, July 1985, pp. 882-897.

8 N.M. Newmark "A method of computation for structural dynamics" J. Eng. Mech. Div. ASCE, vol.85, No.EM3, 1959, pp.67-94.

NATIONAL CENTER FOR EARTHQUAKE ENGINEERING RESEARCH
LIST OF PUBLISHED TECHNICAL REPORTS

The National Center for Earthquake Engineering Research (NCEER) publishes technical reports on a variety of subjects related to earthquake engineering written by authors funded through NCEER. These reports are available from both NCEER's Publications Department and the National Technical Information Service (NTIS). Requests for reports should be directed to the Publications Department, National Center for Earthquake Engineering Research, State University of New York at Buffalo, Red Jacket Quadrangle, Buffalo, New York 14261. Reports can also be requested through NTIS, 5285 Port Royal Road, Springfield, Virginia 22161. NTIS accession numbers are shown in parenthesis, if available.

NCEER-87-0001 "First-Year Program in Research, Education and Technology Transfer," 3/5/87, (PB88-134275/AS).

NCEER-87-0002 "Experimental Evaluation of Instantaneous Optimal Algorithms for Structural Control," by R.C. Lin, T.T. Soong and A.M. Reinhorn, 4/20/87, (PB88-134341/AS).

NCEER-87-0003 "Experimentation Using the Earthquake Simulation Facilities at University at Buffalo," by A.M. Reinhorn and R.L. Ketter, to be published.

NCEER-87-0004 "The System Characteristics and Performance of a Shaking Table," by J.S. Hwang, K.C. Chang and G.C. Lee, 6/1/87, (PB88-134259/AS).

NCEER-87-0005 "A Finite Element Formulation for Nonlinear Viscoplastic Material Using a Q Model," by O. Gyebi and G. Dasgupta, 11/2/87, (PB88-213764/AS).

NCEER-87-0006 "Symbolic Manipulation Program (SMP) - Algebraic Codes for Two and Three Dimensional Finite Element Formulations," by X. Lee and G. Dasgupta, 11/9/87, (PB88-219522/AS).

NCEER-87-0007 "Instantaneous Optimal Control Laws for Tall Buildings Under Seismic Excitations," by J.N. Yang, A. Akbarpour and P. Ghaemmaghami, 6/10/87, (PB88-134333/AS).

NCEER-87-0008 "IDARC: Inelastic Damage Analysis of Reinforced Concrete-Frame Shear-Wall Structures," by Y.J. Park, A.M. Reinhorn and S.K. Kunnath, 7/20/87, (PB88-134325/AS).

NCEER-87-0009 "Liquefaction Potential for New York State: A Preliminary Report on Sites in Manhattan and Buffalo," by M. Budhu, V. Vijayakumar, R.F. Giese and L. Baumgras, 8/31/87, (PB88-163704/AS).

NCEER-87-0010 "Vertical and Torsional Vibration of Foundations in Inhomogeneous Media," by A.S. Veletsos and K.W. Dotson, 6/1/87, (PB88-134291/AS).

NCEER-87-0011 "Seismic Probabilistic Risk Assessment and Seismic Margins Studies for Nuclear Power Plants," by Howard H.M. Hwang, 6/15/87, (PB88-134267/AS).

NCEER-87-0012 "Parametric Studies of Frequency Response of Secondary Systems Under Ground-Acceleration Excitations," by Y. Yong and Y.K. Lin, 6/10/87, (PB88-134309/AS).

NCEER-87-0013 "Frequency Response of Secondary Systems Under Seismic Excitation," by J.A. HoLung, J. Cai and Y.K. Lin, 7/31/87, (PB88-134317/AS).

NCEER-87-0014 "Modelling Earthquake Ground Motions in Seismically Active Regions Using Parametric Time Series Methods," G.W. Ellis and A.S. Cakmak, 8/25/87, (PB88-134283/AS).

NCEER-87-0015 "Detection and Assessment of Seismic Structural Damage," by E. DiPasquale and A.S. Cakmak, 8/25/87, (PB88-163712/AS).

NCEER-87-0016 "Pipeline Experiment at Parkfield, California," by J. Isenberg and E. Richardson, 9/15/87, (PB88-163720/AS).

NCEER-87-0017 "Digital Simulation of Seismic Ground Motion," by M. Shinozuka, G. Deodatis and T. Harada, 8/31/87, (PB88-155197/AS).

NCEER-87-0018 "Practical Considerations for Structural Control: System Uncertainty, System Time Delay and Truncation of Small Control Forces," J. Yang and A. Akbarpour, 8/10/87, (PB88-163738/AS).

NCEER-87-0019 "Modal Analysis of Nonclassically Damped Structural Systems Using Canonical Transformation," by J.N. Yang, S. Sarkani and F.X. Long, 9/27/87, (PB88-187851/AS).

NCEER-87-0020 "A Nonstationary Solution in Random Vibration Theory," by J.R. Red-Horse and P.D. Spanos, 11/3/87, (PB88-163746/AS).

NCEER-87-0021 "Horizontal Impedances for Radially Inhomogeneous Viscoelastic Soil Layers," by A.S. Veletsos and K.W. Dotson, 10/15/87, (PB88-150859/AS).

NCEER-87-0022 "Seismic Damage Assessment of Reinforced Concrete Members," by Y.S. Chung, C. Meyer and M. Shinozuka, 10/9/87, (PB88-150867/AS).

NCEER-87-0023 "Active Structural Control in Civil Engineering," by T.T. Soong, 11/11/87, (PB88-187778/AS).

NCEER-87-0024 "Vertical and Torsional Impedances for Radially Inhomogeneous Viscoelastic Soil Layers," by K.W. Dotson and A.S. Veletsos, 12/87, (PB88-187786/AS).

NCEER-87-0025 "Proceedings from the Symposium on Seismic Hazards, Ground Motions, Soil-Liquefaction and Engineering Practice in Eastern North America, October 20-22, 1987, edited by K.H. Jacob, 12/87, (PB88-188115/AS).

NCEER-87-0026 "Report on the Whittier-Narrows, California, Earthquake of October 1, 1987," by J. Pantelic and A. Reinhorn, 11/87, (PB88-187752/AS).

NCEER-87-0027 "Design of a Modular Program for Transient Nonlinear Analysis of Large 3-D Building Structures," by S. Srivastav and J.F. Abel, 12/30/87, (PB88-187950/AS).

NCEER-87-0028 "Second-Year Program in Research, Education and Technology Transfer," 3/8/88, (PB88-219480/AS).

NCEER-88-0001 "Workshop on Seismic Computer Analysis and Design of Buildings With Interactive Graphics," by J.F. Abel and C.H. Conley, 1/18/88, (PB88-187760/AS).

NCEER-88-0002 "Optimal Control of Nonlinear Flexible Structures," J.N. Yang, F.X. Long and D. Wong, 1/22/88, (PB88-213772/AS).

NCEER-88-0003 "Substructuring Techniques in the Time Domain for Primary-Secondary Structural Systems," by G. D. Manolis and G. Juhn, 2/10/88, (PB88-213780/AS).

NCEER-88-0004 "Iterative Seismic Analysis of Primary-Secondary Systems," by A. Singhal, L.D. Lutes and P. Spanos, 2/23/88, (PB88-213798/AS).

NCEER-88-0005 "Stochastic Finite Element Expansion for Random Media," P. D. Spanos and R. Ghanem, 3/14/88, (PB88-213806/AS).

NCEER-88-0006 "Combining Structural Optimization and Structural Control," F. Y. Cheng and C. P. Pantelides, 1/10/88, (PB88-213814/AS).

NCEER-88-0007 "Seismic Performance Assessment of Code-Designed Structures," H.H-M. Hwang, J-W. Jaw and H-J. Shau, 3/20/88, (PB88-219423/AS).

NCEER-88-0008 "Reliability Analysis of Code-Designed Structures Under Natural Hazards," H.H-M. Hwang, H. Ushiba and M. Shinozuka, 2/29/88.

NCEER-88-0009 "Seismic Fragility Analysis of Shear Wall Structures," J-W Jaw and H.H-M. Hwang, 4/30/88.

NCEER-88-0010 "Base Isolation of a Multi-Story Building Under a Harmonic Ground Motion - A Comparison of Performances of Various Systems," F-G Fan, G. Ahmadi and I.G. Tadjbakhsh, 5/18/88.

NCEER-88-0011 "Seismic Floor Response Spectra for a Combined System by Green's Functions," F.M. Lavelle, L.A. Bergman and P.D. Spanos, 5/1/88.

NCEER-88-0012 "A New Solution Technique for Randomly Excited Hysteretic Structures," G.Q. Cai and Y.K. Lin, 5/16/88.

NCEER-88-0013 "A Study of Radiation Damping and Soil-Structure Interaction Effects in the Centrifuge," K. Weissman, supervised by J.H. Prevost, 5/24/88.

NCEER-88-0014 "Parameter Identification and Implementation of a Kinematic Plasticity Model for Frictional Soils," J.H. Prevost and D.V. Griffiths, to be published.

NCEER-88-0015 "Two- and Three-Dimensional Dynamic Finite Element Analyses of the Long Valley Dam," D.V. Griffiths and J.H. Prevost, 6/17/88.

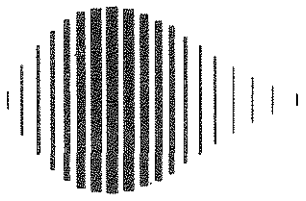

National Center for Earthquake Engineering Research
State University of New York at Buffalo